Aerospace Science and Technology 155 (2024) 109561

Contents lists available at ScienceDirect

Aerospace Science and Technology

journal homepage: www.elsevier.com/locate/aescte

NURBS-based isogeometric formulation for linear and nonlinear buckling analysis of laminated composite plates using constrained and unconstrained TSDTs

Surendra Verma [a,*], Abha Gupta [b], Rabindra Prasad [c], Donatus Oguamanam [a]

[a] Department of Mechanical, Industrial, and Mechatronics Engineering, Toronto Metropolitan University, Toronto, Ontario M5B 2K3, Canada
[b] Department of Aerospace Engineering, Punjab Engineering College (DU), Chandigarh 160012, India
[c] Mechanical Engineering Department, Indian Institute of Information Technology Design & Manufacturing Jabalpur, Jabalpur, Madhya Pradesh 482005, India

ARTICLE INFO

Communicated by Duc Dinh Nguyen

Keywords:
Nonlinear buckling analysis
Isogeometric analysis
Green-Lagrange nonlinearity
von Kármán nonlinearity
High-order plate theory
Pre-buckling boundary conditions

ABSTRACT

Two isogeometric plate models employing Reddy's third-order shear deformation theory (TSDT) and unconstrained third-order shear deformation theory (UTSDT) are presented and compared for linear and nonlinear buckling analysis of laminated composite plates with and without imperfection and subjected to different in-plane loads. Cubic non-uniform rational B-spline (NURBS) basis functions that easily satisfy C^1 continuity of the IGA-TSDT model are employed. The total Lagrangian approach in conjunction with the principle of virtual work is used to derive the governing equations. The primary and secondary solutions are traced using a tangent based arc-length method with a simple branch switching technique. The performance of the models is evaluated by validation and comparison with solutions obtained using ANSYS, Navier method (for linear analysis only), and those in the literature. The buckling response is significantly affected by pre-buckling boundary conditions and strain-displacement relations. The nonlinear buckling approach, among other approaches, is observed to be the most accurate methodology for an arbitrarily laminated composite plate. Further, IGA-UTSDT with nine DOF gives marginal improvement over IGA-TSDT with five DOF at the cost of computation. The IGA-TSDT is observed to be superior to FEM-TSDT in terms of computation demand and performance.

1. Introduction

Composite materials are increasing used in various industries, including aerospace, automotive, defense, railways, shipbuilding, and polymeric electronics, due to their high specific strength and stiffness characteristics. In aerospace engineering specifically, laminated composites structures are widely used in the form of beams, plates, and panels, finding use in wing spars, wing skins, fuselage, bulkheads, control surfaces, flaps, spoilers, gusset plates, and airframes.

In a previous paper [1], a penalty based C^0 finite element model with seven degrees of freedom (DOF) is proposed for a C^1 high-order shear deformation theory (HSDT), particularly Reddy's third-order shear deformation theory (TSDT), for linear and nonlinear buckling analysis of laminated composite plates. The limitation of C^0 continuous Lagrange elements not only introduced approximation to the solution but also increased the computational cost because of the penalty approach. The present study is an attempt to improve the model using isogeometric analysis (IGA).

IGA technique, proposed by Hughes et al. [2], ensures C^1 requirement of HSDT and requires less computation power due to the use of non-uniform rational B-splines (NURBS). In addition, IGA provides a seamless integration of computer-aided design (CAD) and computer-aided engineering (CAE) and allows the analysis to be implemented on the geometry with higher continuity, instead of the conventional finite element mesh with C^0 continuity.

Many linear studies [3–11] predict the buckling strength of composite plates under inplane mechanical loads. Most of these studies [1,3–6,10,11] use the finite element method, and it is worth noticing that [1,3,7–9] found that the use of Green-Lagrange strain yields accurate prediction of buckling strength. Refs. [12–18] employ the IGA technique. Specifically, the IGA is combined with first-order shear deformation theory (FSDT)

* Corresponding author.
E-mail addresses: suri@torontomu.ca, surendraverma2501@gmail.com (S. Verma), abha.gupta91@gmail.com (A. Gupta), rabindrap@iiitdmj.ac.in (R. Prasad), doguaman@torontomu.ca (D. Oguamanam).

https://doi.org/10.1016/j.ast.2024.109561
Received 2 June 2024; Received in revised form 4 September 2024; Accepted 4 September 2024
Available online 10 September 2024

[12,13], TSDT [14,15], non-polynomial shear deformation theory (NPSDT) [16,17], and layer-wise theory [18]. Other noteworthy studies include that by Le-Manh and Lee [19] which is based on IGA-FSDT and employs genetic algorithm and assumed stress approach to optimize ply sequence for maximum buckling strength. The normal inplane displacements are unconstrained and result in uniform stress distribution. Shojaee et al. [20] and Yu et al. [21,22] use a level-set method to investigate the effects of cutouts on buckling strength of laminated composite plates; IGA-CLPT (classical laminated plate theory) [20,21] and IGA-FSDT [22] models are used with von Kármán strain nonlinearity. The IGA is used with the fourth-order Carrera's Unified Formulation by Alesadi et al. [23] to examine buckling behavior of cross-ply laminated composite plates; uniform stress distribution is assumed, and von Kármán strain nonlinearity is employed. Nguyen et al. [24] use a simplified IGA-NPSDT model to examine the effect of uncertainty in Young's modulus on the buckling strength of laminated composite plates. The formulation uses assumed stress approach with von Kármán strain nonlinearity. A similar analysis is reported by Atri and Shojaee [25] while employing a TSDT model with basis functions that are generated with truncated hierarchical B-Spline with reproducing kernal particle method. The IGA collocation method is extended to the buckling analysis of symmetric cross-ply laminated plates in Ref. [26] where FSDT model is employed while excluding inplane displacements. A uniform stress distribution is assumed, and geometric stiffening is captured via the use of von Kármán strain nonlinearity.

Similar to finite element studies, as reviewed in [1], most of the IGA-based studies assume uniform stress distribution, which is an oversimplified approximation. The assumed stress approach is also extended to problems [20–22] that contain geometric discontinuity such as cutouts. Some studies consider a two-stage analysis approach in which stress distribution is calculated in a pre-buckling stage and later utilized in eigenvalue approach to the calculate buckling strength. The key factor in the two-stage analysis is the type of boundary conditions employed in the pre-buckling analysis. While numerous studies [27–33] employ pre-buckling boundary conditions which yield almost uniform stress distribution, much like in the assumed stress approach, few studies [1,5,32,34] consider identical boundary conditions in the two-stage analysis which encapsulate the non-uniform stress distribution. Regarding stress and strain loading, Prajapati et al. [35] and Alhajahmad and Mittelstedt [36] observe that a plate with a constant strain loading has higher buckling strength than one with constant stress loading, implying that conservative designs could be obtained by using constant stress loading, and it is the loading option employed in this study. It is observed that plates/panels with imperfections [19,37] and structures with bending-stretching coupling or partial edge loading are not buckling problems.

Plates under inplane mechanical loads do not lose their entire stability even beyond the magnitude of their initial buckling strength but follow a secondary path, i.e., a post-buckling path [38,39], that still have the strength due to the effect of nonlinear strain-displacement relationship. The nonlinear buckling analysis [40–44] not only predicts the initial buckling strength but also gives the equilibrium path, limit load, and other details that cannot be gleaned from a linear buckling analysis. Many nonlinear buckling analyses [1,6,45–50] use FSDT [6,46,51], TSDT [1,45,48], and high-order shear and normal deformation theory [49] via FEM. There are also IGA-based studies on the nonlinear buckling analysis of laminated composite plates subjected to inplane loads: Le-Manh and Lee [19] report analyses with and without imperfection – they use FSDT with small rotation Green-Lagrange and von Kármán strain nonlinearity; Tran and Kim [50] investigate the effects of initial imperfection on the buckling and post-buckling behaviors of multilayered plates by employing FSDT and von Kármán strain nonlinearity; Praciano et al. [52] examine plates and shallow shells using FSDT and von Kármán strain nonlinearity. The loading condition used in Ref. [52] is a uniform displacement which is different from a uniform loading. None of these studies examine the efficacy and fidelity of a HSDT model. Further, it is plausible to conclude, on the evidence of the literature, that there are very few comprehensive studies on the efficacy of using the nonlinear eigenvalue approach in tracing post-buckling equilibrium paths, especially for IGA. While, most of the studies are limited to the use of the von Kármán nonlinearity, Refs. [1,19,45] find Green-Lagrange strain nonlinearity to be more reliable and conservative. The literature lacks Green-Lagrange nonlinearity based studies that provide clarity on the consequences of using each nonlinearity formulation, Green-Lagrange or von Kármán.

This study is an attempt to fill the identified knowledge gaps or shortfalls. It presents a comprehensive investigation of the buckling behavior of laminated composite plates subjected to inplane mechanical loads using isogeometric plate models based on TSDT and unconstrained third-order shear deformation theory (UTSDT) identified hereinafter as IGA-TSDT and IGA-UTSDT, respectively. Cubic NURBS basis functions are used, and buckling responses are obtained using the tangent based arc-length solution method in conjunction with a simple branch switching technique [52]. The significance of using consistent boundary conditions and Green-Lagrange strain nonlinearity over the pre-buckling boundary conditions and von Kármán strain nonlinearity is highlighted. And the importance of pre-buckling boundary conditions and solution methodology (or approach) for an accurate and reliable buckling analysis is demonstrated. The simulation results indicate that the accuracy of the nonlinear buckling approach is more reliable than that of the other approaches. Further, the same boundary conditions must be used in the two-stage linear buckling analysis incorporating Green-Lagrange type strain-displacement relationship. Further, the IGA-UTSDT model shows marginally improvement over IGA-TSDT model at the cost of significant computation cost. The IGA-TSDT is found to be superior to FEM-TSDT in both performance and computation efficacy.

A brief overview of the different aspects of IGA is provided in Section 2, and Section 3 contains the isogeometric formulation for buckling problems of laminated composite plates subjected to inplane mechanical loads. The accuracy and efficacy of the proposed C^2 IGA-TSDT and IGA-UTSDT models for buckling analysis are examined in Section 4 through several validation and parametric numerical experiments. Some concluding remarks are provided in Section 5.

2. A brief introduction about isogeometric method

In CAD, geometric objects (curves, surfaces, or volumes) are expressed as a linear combination of control points and basis functions. An important component of basis functions is the knot vector which discretizes the geometric object using parametric coordinates that are listed in it.

2.1. Knot vector

Knot vector $\mathcal{H} = \left\{ \xi_1 \;\; \xi_2 \;\; \cdots \;\; \xi_{n+p+1} \right\}$ is a set of non-decreasing numbers in a parametric space, where p and n are the polynomial degree and number of basis functions corresponding to control point, respectively. Elements of the knot vector are called knots and identified by the symbol ξ_i. Knot intervals, $\left[\xi_i, \xi_{i+1}\right]$ where $\xi_i \neq \xi_{i+1}$, are analogous to finite elements. In general, the knot vector takes values between zero and one, i.e., $0 \leq \xi_i \leq 1$. The segment of the parametric space that defines a knot vector is called a patch. A simple geometry like a plate can be sufficiently parameterized by a single patch. In this study, open knot vectors in which the first and last knots are repeated $p+1$ times are used, which provide Kronecker delta property at the boundaries.

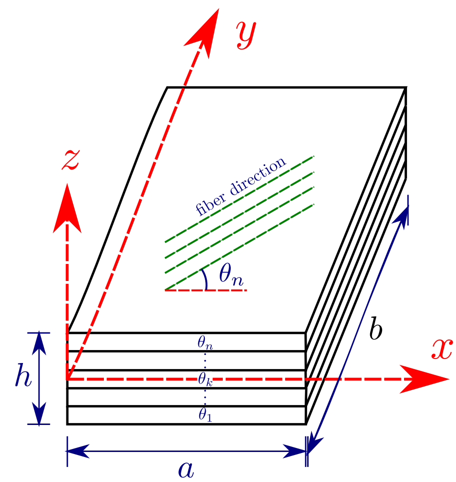

Fig. 1. Schematic diagram of a composite plate with global Cartesian coordinate system (x, y, z).

2.2. B-spline basis functions

For a given knot vector, B-spline basis functions $N^b_{i,p}(\xi)$ of degree $p = 0$ are defined as $N^b_{i,0}(\xi) = \begin{cases} 1 & \xi_i \le \xi < \xi_{i+1} \\ 0 & \text{otherwise} \end{cases}$. The basis function of degree $p > 0$ is defined by Cox-de Boor [2] recursion formula as $N^b_{i,p}(\xi) = \frac{\xi-\xi_i}{\xi_{i+p}-\xi_i} N^b_{i,p-1}(\xi) + \frac{\xi_{i+p+1}-\xi}{\xi_{i+p+1}-\xi_{i+1}} N^b_{i+1,p-1}(\xi)$. A B-spline basis function is C^{p-1} continuous at a single knot. A knot value that appears more than once is called a multiple knot. At a knot of multiplicity $\hat{k}$, the continuity is reduced to $C^{p-\hat{k}}$. The repeated first and last knots in the open knot vector make it easier to implement displacement boundary conditions by satisfying the Kronecker delta property.

2.3. B-spline curves and surfaces

A B-spline curve may be written as $C(\xi) = \sum_{i=1}^{n} N^b_{i,p}(\xi) P_i$, where $P_i = \{x_i, y_i, z_i\}$ is the i^{th} control point and $N^b_{i,p}(\xi)$ is the p^{th} degree B-spline basis function defined over the knot vector $\mathcal{H}$. Further, a B-spline surface is defined by the tensor product of B-spline curves in two parametric dimensions ξ and η with two knot vectors $\mathcal{H}_1 = \{\, \xi_1 \;\; \xi_2 \;\; \cdots \;\; \xi_{n+p+1} \,\}$ and $\mathcal{H}_2 = \{\, \eta_1 \;\; \eta_2 \;\; \cdots \;\; \eta_{m+q+1} \,\}$, respectively. The parametric expression of a B-spline surface may be given as $S(\xi, \eta) = \sum_{i=1}^{n} \sum_{j=1}^{m} N^b_{i,p}(\xi) M^b_{j,q}(\eta) P_{ij} = \sum_{k=1}^{n\times m} N^b_k(\xi, \eta) P_k$ where $N^b_k(\xi, \eta) = N^b_{i,p}(\xi) M^b_{j,q}(\eta)$ is a two-dimensional (2D) B-spline basis function associated with control point k.

2.4. NURBS surfaces

NURBS curves and surfaces are the generalization of B-spline curves and surfaces, respectively. NURBS basis functions are obtained by augmenting every control point P_k with non-negative weight w_k, i.e., $P_k = \{x_k, y_k, z_k, w_k\}$. NURBS surfaces are then defined by $S(\xi, \eta) = \frac{\sum_{k=1}^{n\times m} N^b_k(\xi,\eta) w_k}{\sum_{j=1}^{n\times m} N^b_j(\xi,\eta) w_j} P_k = \sum_{k=1}^{n\times m} R_k(\xi, \eta) P_k$. The first and second derivative of NURBS basis functions $R_k(\xi, \eta)$ used in the isogeometric formulation can be found in Ref. [53] or in standard text on IGA [2]. For a flat plate, an equal weight is considered for all the control points, i.e., unit weight.

2.5. Refinement

The NURBS curves and surfaces can be enriched by three types of refinements [2]: (i) h-refinement (knot insertion); (ii) p-refinement (degree elevation), and (iii) k-refinement (degree elevation then knot insertion), which does not have an equivalent in finite element method. In k-refinement, p-refinement is followed by h-refinement. The advantage of k-refinement is that it yields a smaller number of basis functions with higher inter-element continuity. In the present study, the open source library GeoPDE [54] is utilized to build an initial or coarse geometry. Then, k-refinement is performed using degree elevation and knot insertion functions.

3. Mathematical formulation

Consider a rectangular composite plate with Cartesian coordinate system (x, y, z) such that the xy plane is the midplane of the plate and the z-axis is pointing in the direction of increasing ply numbering as shown in Fig. 1. The plate is composed of n elastic orthotropic layers, stacked in a particular sequence $(\theta_1/\theta_2/\theta_3/\theta_4/\ldots)$ with side length a, width b, and uniform thickness h.

3.1. High-order shear deformation theory

The displacement field corresponding to the TSDT is given as

$$\begin{aligned} u(x,y,z) &= u_0(x,y) - z\frac{\partial w_0}{\partial x} + f(z)\theta_x(x,y) \\ v(x,y,z) &= v_0(x,y) - z\frac{\partial w_0}{\partial y} + f(z)\theta_y(x,y) \\ w(x,y,z) &= w_0(x,y) \end{aligned} \tag{1}$$

where u, v, and w are components of the displacement vector of a generic point in x, y, and z directions, respectively; u_0, v_0, and w_0 are the corresponding midplane displacements; θ_x and θ_y are the shear deformation of the normal to the midplane about the y-axis and x-axis, respectively; and $f(z) = z - 4z^3/3h^2$ denotes the transverse shear function. Different types of polynomial and non-polynomial shear deformation theories (PSDT and NPSDT) can be obtained by changing the function $f(z)$. The displacement field for the UTSDT is given as

$$\begin{aligned} u(x,y,z) &= u_0(x,y) + z\phi_x(x,y) + z^2\theta_x(x,y) + z^3\psi_x \\ v(x,y,z) &= v_0(x,y) + z\phi_y(x,y) + z^2\theta_y(x,y) + z^3\psi_y \\ w(x,y,z) &= w_0(x,y) \end{aligned} \tag{2}$$

where u_0, v_0, and w_0 are midplane components of the displacements in x, y, and z directions, respectively; ϕ_x and ϕ_y are linear components; θ_x and θ_y are quadratic components; and ψ_x and ψ_y are cubic components of displacements u and v in x and y directions, respectively. Note that TSDT enforces zero shear at the top and bottom surfaces.

For the sake of brevity, the isogeometric formulation pertaining to TSDT is briefly discussed in the following section as prominent vectors and matrices of the isogeometric formulation are discussed in an earlier work [53]. IGA formulation using TSDT requires C^1 continuity of the deflection, while UTSDT requires C^0 continuity. The isogeometric formulation using UTSDT is similar to finite element formulation as discussed in Ref. [31] with von Kármán non-linearity. The important vectors and matrices for Green-Lagrange nonlinearity in the framework of UTSDT are given in the appendix.

3.2. Strain-displacement relation

The strain vector $\boldsymbol{\varepsilon}$ using Green-Lagrange strain relation is expressed as

$$\boldsymbol{\varepsilon} = \boldsymbol{\varepsilon_l} + \frac{1}{2}\boldsymbol{\varepsilon_{nl}} + \boldsymbol{\varepsilon}^* \tag{3}$$

in which

$$\boldsymbol{\varepsilon}_l = \left\{ \begin{array}{c} \frac{\partial u}{\partial x} \\ \frac{\partial v}{\partial y} \\ \frac{\partial u}{\partial y} + \frac{\partial v}{\partial x} \\ \frac{\partial v}{\partial z} + \frac{\partial w}{\partial y} \\ \frac{\partial u}{\partial z} + \frac{\partial w}{\partial x} \end{array} \right\}; \boldsymbol{\varepsilon}_{nl} = \left\{ \begin{array}{c} \left(\frac{\partial u}{\partial x}\right)^2 + \left(\frac{\partial v}{\partial x}\right)^2 + \left(\frac{\partial w}{\partial x}\right)^2 \\ \left(\frac{\partial u}{\partial y}\right)^2 + \left(\frac{\partial v}{\partial y}\right)^2 + \left(\frac{\partial w}{\partial y}\right)^2 \\ 2\left(\frac{\partial u}{\partial x}\frac{\partial u}{\partial y} + \frac{\partial v}{\partial x}\frac{\partial v}{\partial y} + \frac{\partial w}{\partial x}\frac{\partial w}{\partial y}\right) \\ 2\left(\frac{\partial u}{\partial y}\frac{\partial u}{\partial z} + \frac{\partial v}{\partial y}\frac{\partial v}{\partial z} + \frac{\partial w}{\partial y}\frac{\partial w}{\partial z}\right) \\ 2\left(\frac{\partial u}{\partial x}\frac{\partial u}{\partial z} + \frac{\partial v}{\partial x}\frac{\partial v}{\partial z} + \frac{\partial w}{\partial x}\frac{\partial w}{\partial z}\right) \end{array} \right\}; \boldsymbol{\varepsilon}^* = \left\{ \begin{array}{c} \frac{\partial w}{\partial x}\frac{\partial w^*}{\partial x} \\ \frac{\partial w}{\partial y}\frac{\partial w^*}{\partial y} \\ \frac{\partial w}{\partial x}\frac{\partial w^*}{\partial y} + \frac{\partial w}{\partial y}\frac{\partial w^*}{\partial x} \\ 0 \\ 0 \end{array} \right\}$$

where $\boldsymbol{\varepsilon_l}$, $\frac{1}{2}\boldsymbol{\varepsilon_{nl}}$, and $\boldsymbol{\varepsilon}^*$ are the linear, nonlinear, and imperfection components of the strain vector $\boldsymbol{\varepsilon}$, respectively. The corresponding strain vector for von Kármán nonlinearity is deduced by retaining only deflection terms ($\partial w/\partial x$ and $\partial w/\partial y$) in the nonlinear strain component $\boldsymbol{\varepsilon}_{nl}$. Here, imperfection is measured from the flat plate (shown in Fig. 1), while displacements are measured from the imperfect configuration.

The term $w^*(x,y)$ denotes the imperfection (or initial deflection) in the z direction. The present study is limited to sinusoidal-type imperfections, i.e., $w^* = w_0^* sin(\pi x/a)\, sin(\pi y/b)$ with maximum imperfection w_0^* at the center of the plate. This imperfection profile is equivalent to the first buckling mode obtained from a linear buckling analysis. Thus, the value of the imperfection at the control points is obtained from a linear buckling analysis. Because NURBS basis functions do not satisfy the Kronecker delta property at interior knots, the imperfection $w^*(x,y)$ cannot be directly mapped to control points. To obtain the correct value of imperfection at the control points, the values of each control point must be scaled with respect to a particular point on the plate surface, i.e., center of the plate.

Taking advantage of the orthotropic nature of composite materials in the computation, the strain vector $\boldsymbol{\varepsilon}$ can be decomposed into both inplane and transverse strain components. Similarly, the linear strain vector $\boldsymbol{\varepsilon}_l$ can be decomposed into linear inplane strain vector $\boldsymbol{\varepsilon}_{lb} = \left\{ \frac{\partial u}{\partial x} \;\; \frac{\partial v}{\partial y} \;\; \frac{\partial u}{\partial y} + \frac{\partial v}{\partial x} \right\}^T$ and linear transverse strain vector $\boldsymbol{\varepsilon}_{ls} = \left\{ \frac{\partial v}{\partial z} + \frac{\partial w}{\partial y} \;\; \frac{\partial u}{\partial z} + \frac{\partial w}{\partial x} \right\}^T$ as

$$\boldsymbol{\varepsilon}_l = \boldsymbol{Z}_l\hat{\boldsymbol{\varepsilon}}_l = \left\{ \begin{array}{c} \boldsymbol{\varepsilon}_{lb} \\ \boldsymbol{\varepsilon}_{ls} \end{array} \right\} = \left\{ \begin{array}{c} \boldsymbol{Z}_{lb}\hat{\boldsymbol{\varepsilon}}_{lb} \\ \boldsymbol{Z}_{ls}\hat{\boldsymbol{\varepsilon}}_{ls} \end{array} \right\} \tag{4}$$

Similarly, nonlinear strain vector $\boldsymbol{\varepsilon}_{nl}$ can be reorganized as follows:

$$\boldsymbol{\varepsilon}_{nl} = \boldsymbol{Z}_{nl}\hat{\boldsymbol{\varepsilon}}_{nl} = \left\{ \begin{array}{c} \boldsymbol{\varepsilon}_{nlb} \\ \boldsymbol{\varepsilon}_{nls} \end{array} \right\} = \left\{ \begin{array}{c} \boldsymbol{Z}_{nlb}\hat{\boldsymbol{\varepsilon}}_{nlb} \\ \boldsymbol{Z}_{nls}\hat{\boldsymbol{\varepsilon}}_{nls} \end{array} \right\} = \left\{ \begin{array}{c} \boldsymbol{Z}_{nlb}\boldsymbol{A}_b\boldsymbol{\phi}_b \\ \boldsymbol{Z}_{nls}\boldsymbol{A}_s\boldsymbol{\phi}_s \end{array} \right\} \tag{5}$$

in which

$$\boldsymbol{\phi}_b = \left\{ \frac{\partial u_0}{\partial x} \;\; \frac{\partial u_0}{\partial y} \;\; \frac{\partial v_0}{\partial x} \;\; \frac{\partial v_0}{\partial y} \;\; \frac{\partial w_0}{\partial x} \;\; \frac{\partial w_0}{\partial y} \;\; -\frac{\partial^2 w_0}{\partial x^2} \;\; -\frac{\partial^2 w_0}{\partial y \partial x} \;\; -\frac{\partial^2 w_0}{\partial x \partial y} \;\; -\frac{\partial^2 w_0}{\partial y^2} \;\; \frac{\partial \theta_x}{\partial x} \;\; \frac{\partial \theta_x}{\partial y} \;\; \frac{\partial \theta_y}{\partial x} \;\; \frac{\partial \theta_y}{\partial y} \right\}^T \tag{6a}$$

$$\boldsymbol{\phi}_s = \left\{ -\frac{\partial w_0}{\partial x} \;\; -\frac{\partial w_0}{\partial y} \;\; \theta_x \;\; \theta_y \;\; \frac{\partial u_0}{\partial x} \;\; \frac{\partial u_0}{\partial y} \;\; \frac{\partial v_0}{\partial x} \;\; \frac{\partial v_0}{\partial y} \;\; -\frac{\partial^2 w_0}{\partial x^2} \;\; -\frac{\partial^2 w_0}{\partial y \partial x} \;\; -\frac{\partial^2 w_0}{\partial x \partial y} \;\; -\frac{\partial^2 w_0}{\partial y^2} \;\; \frac{\partial \theta_x}{\partial x} \;\; \frac{\partial \theta_x}{\partial y} \;\; \frac{\partial \theta_y}{\partial x} \;\; \frac{\partial \theta_y}{\partial y} \right\}^T \tag{6b}$$

Generally, $\hat{\boldsymbol{\varepsilon}}_{lb}$ and $\hat{\boldsymbol{\varepsilon}}_{ls}$ are known as linear inplane and linear transverse generalized strain vectors; $\hat{\boldsymbol{\varepsilon}}_{nlb}$ and $\hat{\boldsymbol{\varepsilon}}_{nls}$ as nonlinear inplane and nonlinear transverse generalized strain vectors; and $\boldsymbol{Z}_{lb}$, $\boldsymbol{Z}_{ls}$, $\boldsymbol{Z}_{nlb}$, and $\boldsymbol{Z}_{nls}$ as thickness matrices. The detailed expressions of $\boldsymbol{Z}_{lb}$, $\boldsymbol{Z}_{ls}$, $\hat{\boldsymbol{\varepsilon}}_{lb}$ $\hat{\boldsymbol{\varepsilon}}_{ls}$, $\boldsymbol{Z}_{nlb}$ and $\boldsymbol{Z}_{nls}$ are given in [55]. The expressions of $\boldsymbol{A}_b$ and $\boldsymbol{A}_s$ can be found by isolating $\boldsymbol{\phi}_i$ from the $\hat{\boldsymbol{\varepsilon}}_{nli}$ and they are provided in the appendix for UTSDT.

3.3. Constitutive relation

The constitutive relation for an arbitrary s^{th} orthotropic layer of multilayered plate with zero transverse normal stress condition is given by generalized Hooke' law as

$$\boldsymbol{\sigma} = \bar{\boldsymbol{Q}}^{(s)} \boldsymbol{\varepsilon} = \left[T^{(s)}_{\text{trans}} \right] \boldsymbol{Q}^{(s)} \left[T^{(s)}_{\text{trans}} \right]^T \boldsymbol{\varepsilon} \tag{7}$$

where $\boldsymbol{\sigma}$, $\boldsymbol{\varepsilon}$, and $\bar{\boldsymbol{Q}}$ are stress vector, strain vector, and constitutive matrix in the global Cartesian coordinate system, respectively, while $\boldsymbol{Q}^{(s)}$ denotes the constitutive matrix in the local Cartesian coordinate system. The explicit relation and details of the transformation matrix $T^{(s)}_{\text{trans}}$ and material constant matrix $\boldsymbol{Q}^{(s)}$ can be found in any standard text on composite material or in Ref. [53]. Again by utilizing the property of the orthotropic nature of composite materials, stress vector $\boldsymbol{\sigma} = \left\{ \sigma_{xx} \;\; \sigma_{yy} \;\; \tau_{xy} \;\; \tau_{yz} \;\; \tau_{xz} \right\}^T$ can be decomposed into inplane stress vector $\boldsymbol{\sigma}_b = \left\{ \sigma_{xx} \;\; \sigma_{yy} \;\; \tau_{xy} \right\}^T$ and transverse stress vector $\boldsymbol{\sigma}_s = \left\{ \tau_{yz} \;\; \tau_{xz} \right\}^T$. The generalized inplane stresses and generalized transverse stresses for TSDT are same as defined in [55]. The expressions for generalized stresses for UTSDT are given in the appendix.

3.4. Variational principle

For an admissible virtual displacements $\delta \{u, v, w\}$, the principle of virtual work for the given system, using total Lagrangian approach, may be written as

$$\int_V \{\delta \boldsymbol{\varepsilon}\}^T \{\boldsymbol{\sigma}\} \, dV = \int_s \left(\delta u_0 n_x + \delta v_0 n_y \right) P_i|_{z=0} dS \tag{8}$$

where $P_i(x, y)|_{z=0}$ represents the inplane line loads acting normal to the cross-section area at the reference edge line with n_x and n_y being the direction cosines of the (inplane). Instead of inplane mechanical or edge loading (stress loading), inplane displacement (strain loading) can also be applied to characterize buckling. As suggested in Ref. [35,36], edge loading (stress loading) gives a lower bound to buckling strength, providing a reliable and safe structural design. Hence, the present study deals with inplane mechancial loads only. Further, the present study is limited to dead loads that do not change with the plate deformation, and all kinematics and stresses are measured with respect to the imperfect configuration. The detailed expressions of virtual strain energy and virtual work done by inplane mechanical loads are provided in [1].

3.5. NURBS based discretization

An isoparametric concept is used in IGA to interpolate both geometry and displacement variables ($\boldsymbol{u} = \left\{u_0, v_0, w_0, \theta_x, \theta_y\right\}^T$ for TSDT and $\boldsymbol{u} = \left\{u_0, v_0, w_0, \phi_x, \phi_y, \theta_x, \theta_y, \psi_x, \psi_y\right\}^T$ for UTSDT) using NURBS basis functions. NURBS can reproduce freeform shapes, hence geometry is exactly encapsulated in IGA. Another advantage of NURBS is that it provides higher continuity to displacement variables which limits the DOF to five for TSDT and nine for UTSDT, respectively.

The displacement vector $\boldsymbol{u}$ on the plate surface is interpolated by a linear combination of NURBS basis functions and displacement vectors at the control points $\boldsymbol{q}_k$. For a range of knot intervals, only $p \times q$ NURBS basis functions are non-zero out of $n \times m$ NURBS basis functions. The spatial and field variables are interpolated as

$$x(\xi, \eta) = \sum_{k=1}^{p\times q} R_k(\xi, \eta)\, x_k; \quad y(\xi, \eta) = \sum_{k=1}^{p\times q} R_k(\xi, \eta)\, y_k; \quad \boldsymbol{u}(\xi, \eta) = \sum_{k=1}^{p\times q} R_k(\xi, \eta)\, \boldsymbol{q}_k \tag{9}$$

where $R_k(\xi, \eta)$ and $\boldsymbol{q}_k$ are the (non-zero) NURBS basis function and displacement vector ($\boldsymbol{q}_k = \left\{u_{0k}, v_{0k}, w_{0k}, \theta_{xk}, \theta_{yk}\right\}^T$ for TSDT whereas $\boldsymbol{q}_k = \left\{u_{0k}, v_{0k}, w_{0k}, \phi_{xk}, \phi_{yk}, \theta_{xk}, \theta_{yk}, \psi_{xk}, \psi_{yk}\right\}^T$ for UTSDT) associated with control point k, respectively. The non-zero NURBS basis functions are determined using the Cox-de Boor recursion formula as stated in Section 2.2.

Similar to stress and strain vectors, the strain energy is decomposed into bending and transverse shear components. Using Eq. (9), the generalized strain vector $\hat{\varepsilon}$ can be written in terms of the element strain-displacement matrix $\boldsymbol{B}$ and element displacement vector $\boldsymbol{q}$ as

$$\begin{gathered}\hat{\boldsymbol{\varepsilon}}_{lj} = \sum_{k=1}^{p\times q} \boldsymbol{B}^L_{jk} \boldsymbol{q}_k = \boldsymbol{B}^L_j \boldsymbol{q}; \;\; \hat{\boldsymbol{\varepsilon}}^* = \sum_{k=1}^{p\times q} \boldsymbol{B}^*_k \boldsymbol{q}_k = \boldsymbol{B}^* \boldsymbol{q}; \;\; \hat{\boldsymbol{\varepsilon}}_{nlj} = \sum_{k=1}^{p\times q} \boldsymbol{A}_j \boldsymbol{G}^{NL}_{kj} \boldsymbol{q}_k = \sum_{k=1}^{p\times q} \boldsymbol{B}^{NL}_{jk} \boldsymbol{q}_k = \boldsymbol{B}^{NL}_j \boldsymbol{q} \\ \boldsymbol{q} = \left\{ \boldsymbol{q}_1^T \;\; \boldsymbol{q}_2^T \;\; \cdots \;\; \boldsymbol{q}_{p\times q}^T \right\}^T\end{gathered} \tag{10}$$

where the bending contribution is obtained by substituting $j = b$, and the transverse shear contribution is obtained by substituting $j = s$. The explicit expressions of $\boldsymbol{B}^L_j$, $\boldsymbol{B}^*$ and $\boldsymbol{G}^{NL}_j$ contain terms which require first $\left(\frac{\partial R_k}{\partial x} \text{ and } \frac{\partial R_k}{\partial y} \right)$ and second $\left(\frac{\partial^2 R_k}{\partial x^2}, \frac{\partial^2 R_k}{\partial y^2} \text{ and } \frac{\partial^2 R_k}{\partial x \partial y} \right)$ order derivatives of the NURBS basis R_k. Using chain-rule, Cartesian derivatives of R_k can be calculated from parametric derivative of R_k as discussed in Ref. [53,55].

Table 1
Material properties of laminated composite plates.

Material	E_1 GPa	E_2 GPa	G_{12} GPa	G_{13} GPa	G_{23} GPa	ν_{12} -
MM1 [56–58]	$25E_2$ or Specified	1	$0.5E_2$	$0.5E_2$	$0.2E_2$	0.25
MM2 [58]	$40E_2$ or Specified	1	$0.6E_2$	$0.6E_2$	$0.5E_2$	0.25

3.6. System of equations

By using Eq. (10) and Eq. (9) in Eq. (8), and then eliminating virtual displacement vector $(\delta \boldsymbol{q})^T$, the set of governing equations for nonlinear buckling analysis of composite plates is obtained as

$$\boldsymbol{K}\boldsymbol{q} = \boldsymbol{F}_P \tag{11}$$

where $\boldsymbol{K}$ and $\boldsymbol{F}_P$ represent the force vector due to inplane mechanical loads and nonlinear stiffness matrix, respectively. These are written in expanded form as

$$\boldsymbol{K} = \int_V \left(\left(\boldsymbol{B}^L + \boldsymbol{B}^*\right)^T \boldsymbol{Z}_l^T \bar{\boldsymbol{Q}} \boldsymbol{Z}_l \left(\boldsymbol{B}^L + \boldsymbol{B}^*\right) + \frac{1}{2}\left(\boldsymbol{B}^L + \boldsymbol{B}^*\right)^T \boldsymbol{Z}_l^T \bar{\boldsymbol{Q}} \boldsymbol{Z}_{nl} \boldsymbol{B}^{NL} + \left(\boldsymbol{B}^{NL}\right)^T \boldsymbol{Z}_{nl}^T \bar{\boldsymbol{Q}} \boldsymbol{Z}_l \left(\boldsymbol{B}^L + \boldsymbol{B}^*\right) + \frac{1}{2}\left(\boldsymbol{B}^{NL}\right)^T \boldsymbol{Z}_{nl}^T \bar{\boldsymbol{Q}} \boldsymbol{Z}_{nl} \boldsymbol{B}^{NL} \right) dz\, dA \tag{12a}$$

$$\boldsymbol{F}_P = \int_s \{\mathcal{U}\}^T P_i(x,y)\, ds \quad \text{with} \quad \{\mathcal{U}\}\{\boldsymbol{q}\} = \sum_{k=1}^{p\times q} \{\mathcal{U}_k\} \boldsymbol{q}_k \tag{12b}$$

where $\{\mathcal{U}_k\} = \{\, n_x R_k \;\; n_y R_k \;\; 0 \;\; 0 \;\; 0 \,\}$ for TSDT and $\{\mathcal{U}_k\} = \{\, n_x R_k \;\; n_y R_k \;\; 0 \;\; 0 \;\; 0 \;\; 0 \;\; 0 \;\; 0 \;\; 0 \,\}$ for UTSDT.

The solution procedure for Eq. (11) follows [1], with the expressions of $\mathbb{N}_b$ and $\mathbb{N}_s$ for TSDT given in Ref. [53] and those of $\mathbb{N}_b$ and $\mathbb{N}_s$ for UTSDT given in the appendix. Two types of analyses are conducted, namely, linear buckling analysis either using pre-buckling approach or linear buckling approach, and nonlinear buckling analysis using either nonlinear eigenvalue approach (eigenvalue analysis augmented with nonlinear stiffness) or nonlinear buckling approach (solving Eq. (11)). The detailed steps of each approach are discussed in [1] and the applied loads are line loads, i.e., $P_i = N_{xx}$. The set of governing equations for linear buckling analysis of composite plates is given by pre-buckling analysis:

$$\boldsymbol{K}_1 \boldsymbol{q}_s = \boldsymbol{F}_P \tag{13}$$

with $\boldsymbol{K}_1 = \int_V \left(\left(\boldsymbol{B}^L\right)^T \boldsymbol{Z}_l^T \bar{\boldsymbol{Q}} \boldsymbol{Z}_l \left(\boldsymbol{B}^L\right) \right) dz\, dA$ and followed by eigenvalue analysis:

$$\left(\boldsymbol{K}_1\right) \boldsymbol{q}_d - \lambda \boldsymbol{K}_\sigma \left(\boldsymbol{q}_s\right) \boldsymbol{q}_d = 0$$

where $\boldsymbol{q}_d$ is the mode shape corresponding to the eigenvalue (or buckling load) and $\boldsymbol{K}_\sigma\left(\boldsymbol{q}_s\right)$ is the geometric stiffness matrix. The stress-resultants used in $\boldsymbol{K}_\sigma\left(\boldsymbol{q}_s\right)$ are defined by linear stress-strain relationship. The derivation of $\boldsymbol{K}_\sigma\left(\boldsymbol{q}_s\right)$ is given in Ref. [53]. The critical buckling load is obtained by multiplying the critical load multiplier λ with the base load, i.e., the unit load in the pre-buckling analysis, Eq. (13).

4. Results and discussions

In this section, the two IGA models, namely, IGA-TSDT and IGA-UTSDT, are employed for various buckling problems of laminated composite plates to assess the accuracy and reliability of each buckling approach. The stiffening effect of applied loads is captured by considering von Kármán or Green-Lagrange strain-displacement relationship. The numerical investigations are categorized as either linear or nonlinear. Studies are conducted to observe the effect of side-to-thickness ratio b/h, Young's modulus ratio E_1/E_2, aspect ratio a/b, fiber orientation θ, stacking sequencing, boundary conditions, and different types of inplane loads.

For IGA solutions, a cubic order NURBS element ($p = 3$ and $q = 3$) is used with 14×14 element mesh. To accomplish this, two computer programs, one for IGA-TSDT and the other for IGA-UTSDT, are written in MATLAB with GeoPDEs library. GeoPDEs library has a collection of functions such as *nrbmak*, *nrbdegelev*, and *nrbkntins* for the construction of the plate geometry, and implementation of k-refinement (p-refinement followed by h-refinement) [54], respectively. For numerical calculations, a selective Gauss-Legendre quadrature rule is used: $(p+1)\times(q+1)$ Gauss-Legendre quadrature rule for linear bending stiffness and force vector, and $p\times q$ Gauss-Legendre quadrature rule for linear transverse stiffness and all remaining terms. It is worth mentioning that the present formulation using cubic NURBS elements with k-refinement and selective integration does not exhibit shear locking.

The obtained IGA results are also validated against available solutions in the literature along with Navier and ANSYS solutions. The Navier solution for linear buckling analysis is based on the assumed stress approach, i.e., assumption of uniform stress. A comprehensive formulation of Navier solution for TSDT and UTSDT is presented in the appendix of Ref. [1] and Appendix D, respectively.

4.1. Material properties

It is assumed that the thickness of each ply is equal and constant, and they have identical properties as tabulated in Table 1.

4.2. Boundary conditions

The present IGA formulation is based on the displacement approach, hence only kinematics boundary conditions are constrained along the edges of plates. The different types of boundary conditions used in the present study for TSDT are listed as follows:

- Pre-buckling
  $w_0 = \phi_x = 0$ at $y = 0, b$ and $w_0 = \phi_y = 0$ at $x = 0, a$ for simply supported constraints
  $w_0 = \frac{\partial w_0}{\partial x} = \frac{\partial w_0}{\partial y} = \phi_x = \phi_y = 0$ at $y = 0, b$ and $x = 0, a$ for clamped constraints
  Tying conditions: $u_0 = v_0 = 0$ at $(x = 0, y = 0)$ and $v_0 = 0$ at $(x = a, y = 0)$
  Tying conditions are used to restrict rigid motion in the pre-buckling analysis.
- Simply supported SSSS
  $u_0 = w_0 = \phi_x = 0$ at $y = 0, b$ and $v_0 = w_0 = \phi_y = 0$ at $x = 0, a$
- Clamped CCCC
  $u_0 = v_0 = w_0 = \frac{\partial w_0}{\partial x} = \frac{\partial w_0}{\partial y} = \phi_x = \phi_y = 0$ at $y = 0, b$ and $x = 0, a$
- ABFD
  A at $y = 0$, B at $x = b$, no condition (free) at $y = b$, D at $x = 0$

The deflection is made zero along the control points adjacent to boundary control points to constrain the slope across the boundary.

Similarly, the different types of boundary conditions for UTSDT are listed as follows:

- Pre-buckling
  $w_0 = \phi_x = \theta_x = \psi_x = 0$ at $y = 0, b$ and $w_0 = \phi_y = \theta_y = \psi_y = 0$ at $x = 0, a$ for simply supported constraints
  $w_0 = \phi_x = \phi_y = \theta_x = \theta_y = \psi_x = \psi_y = 0$ at $y = 0, b$ and $x = 0, a$ for clamped constraints
  Tying conditions: $u_0 = v_0 = 0$ at $(x = 0, y = 0)$ and $v_0 = 0$ at $(x = a, y = 0)$
  Tying conditions are used to restrict rigid motion in the pre-buckling analysis.
- Simply supported SSSS
  $u_0 = w_0 = \phi_x = \theta_x = \psi_x = 0$ at $y = 0, b$ and $v_0 = w_0 = \phi_y = \theta_y = \psi_y = 0$ at $x = 0, a$
- Clamped CCCC
  $u_0 = v_0 = w_0 = \phi_x = \phi_y = \theta_x = \theta_y = \psi_x = \psi_y = 0$ at $y = 0, b$ and $x = 0, a$

4.3. Linear buckling analysis

In present study, three linear buckling approaches are identified and named according to the boundary conditions employed in the linear static analysis. The approach in which pre-buckling boundary conditions are used is called pre-buckling approach; linear buckling approach uses the same boundary conditions as used in linear buckling analysis; the assumed stress approach assumes uniform stress distribution and does not require a linear static analysis. The applied inplane mechanical loads in the buckling analysis are mostly inplane line loads perpendicular to the edge or stress resultants, i.e., $P_i = N_{xx}$. The different types of inplane mechanical loads considered are illustrated in Fig. 2.

4.3.1. Effect of side-to-thickness ratio b/h

In this problem, the effect of side-to-thickness ratio b/h on the buckling characteristics of laminated composite plates is investigated via the use of a simply supported (SSSS) square cross-ply laminated plate with material MM1 [58] and subjected to uniform uniaxial loads. The normalized buckling loads $\bar{P} = Pb^2/E_2h^3$ for symmetric and anti-symmetric cross-ply laminated composite plates for different side-to-thickness ratio b/h are tabulated in Table 2. The present IGA-TSDT and IGA-UTSDT solutions are obtained for both von Kármán and Green-Lagrange nonlinearities, and a comparison is made between IGA solutions using assumed stress, pre-buckling, and linear buckling approaches along with ANSYS solutions [1] and Navier solutions.

It is observed that the normalized buckling load $\bar{P}$ decreases with increasing plate thickness while the dimensional buckling load P increases. A good agreement is found between the pre-buckling and assumed stress approaches for symmetric cross-ply laminated composite plates, when von Kármán nonlinearity is employed. The buckling loads obtained using the linear buckling approach are higher than those predicted by the pre-buckling approach by approximately 3 to 4%. The results show that the IGA-UTSDT underestimates the buckling load of symmetric cross-ply laminated plates.

The IGA-TSDT underestimates the value for anti-symmetric cross-ply laminated plates however its relevance is invalid as no bifurcation is seen in Section 4.4.3. It is also noted that the IGA-UTSDT solutions are closer to ANSYS solutions [1]. While the difference between IGA-TSDT and IGA-UTSDT solutions is less than 1%, giving IGA-TSDT a computational advantage, it is acknowledged that the difference could be significant in some design and analysis problems. Thus, IGA-UTSDT is recommended for problems where a high accuracy is desired or sensitivity in the buckling load is high. The IGA solutions using von Kármán nonlinearity are higher than those obtained using Green-Lagrange nonlinearity. This highlights the significance of Green-Lagrange stress stiffening for a reliable analysis and safe design of composite plate structures.

4.3.2. Effect of Young's modulus ratio E_1/E_2

The effect of Young's modulus ratio E_1/E_2 on the buckling characteristics of cross-ply laminated composite plates is investigated in this section. A simply supported (SSSS) moderately thick ($a/h = 10$) square cross-ply laminated plates subjected to uniform uniaxial loads is employed. The material properties of each ply correspond to MM2 [58] (listed in Table 1). Table 3 presents the value of normalized buckling load for different buckling approaches as E_1/E_2 ratio varies from 3 to 40. A comparison has been made between IGA-TSDT and IGA-UTSDT in conjunction with von Kármán and Green-Lagrange stress stiffening. As expected, increasing the Young's modulus ratio E_1/E_2 increases the buckling load of the composite plate due to the increase in the bending stiffness of the plate. The difference between the normalized buckling loads using von Kármán stress stiffening and Green-Lagrange stress stiffening is approximately 2%.

It is observed that the buckling loads using the linear buckling approach are higher than those obtained using pre-buckling approach, with the difference ranging from approximately 3% to 35%. This higher buckling load may be attributed to the non-uniform stress distribution generated due to clamped boundary conditions at the plate corners. An identical difference is observed in the nonlinear buckling analysis (as shown in Sections 4.4.1 and 4.4.2). Further, the IGA-UTSDT solutions with Green-Lagrange stress stiffening are observed to be closer to ANSYS solutions [1] than IGA-TSDT solutions with Green-Lagrange stress stiffening. While the difference between the IGA-UTSDT and IGA-TSDT solutions is less than 1%, the computational advantage of IGA-TSDT cannot be overemphasized. The IGA-UTSDT is suggested for problems that require high accuracy due to their sensitivity.

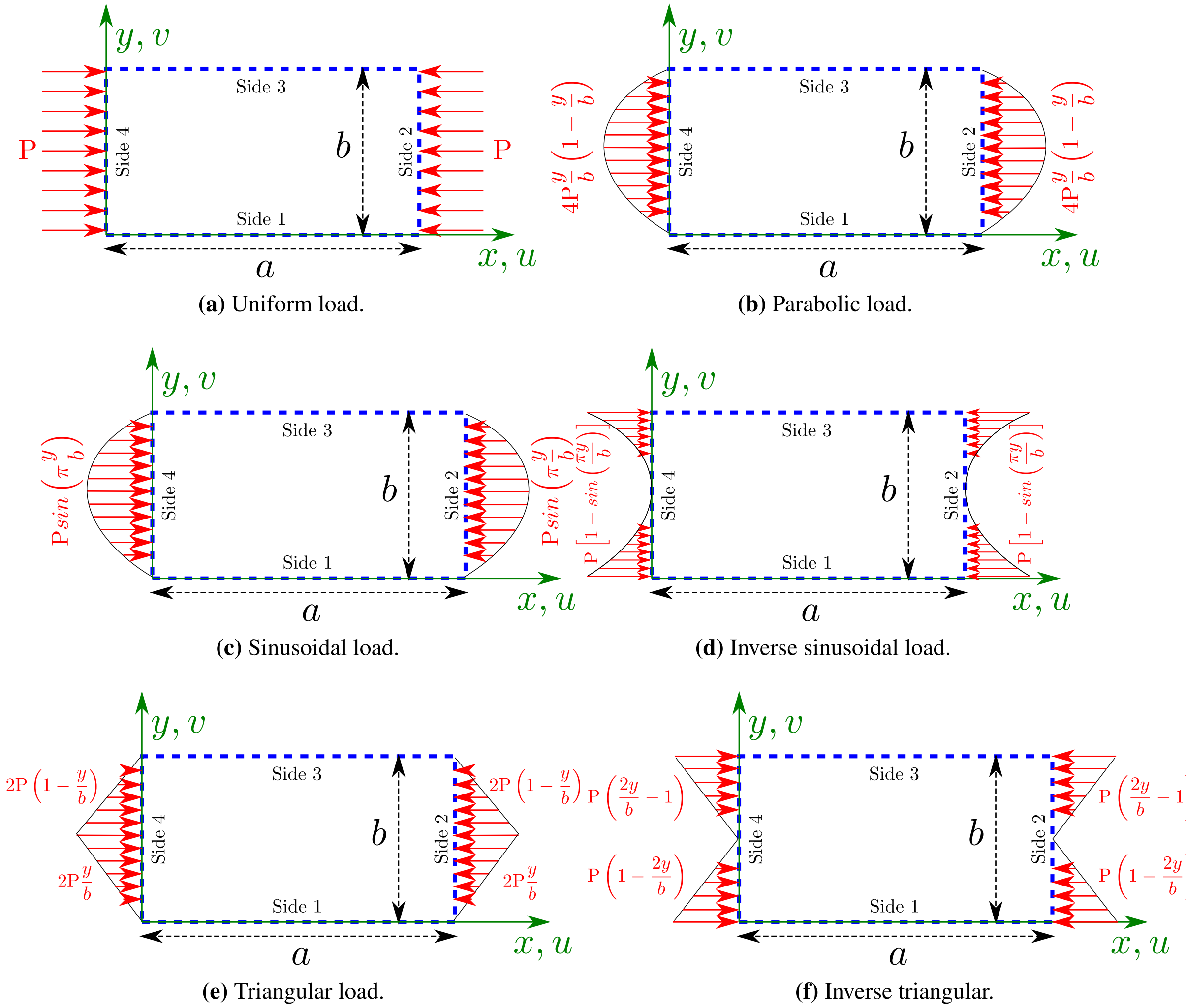

Fig. 2. Different type of uniaxial loads.

4.3.3. *Effect of boundary conditions*

This numerical simulation investigates the effect of different boundary conditions on buckling characteristics of laminated composite plates using IGA-TSDT model. A four-ply (0°/90°/90°/0°) square laminated plate under different combinations of simply supported (S), clamped (C) and free (F) boundary conditions is considered. The material properties are identical to those presented in Section 4.3.2. Two types of inplane load configurations are considered and named as Case-1 (uniaxial compression) and Case-2 (biaxial compression). Tables 4 to 6 show the values of normalized buckling loads $\bar{P} = Pb^2/E_2h^3$ for $a/h = 10$ using both pre-buckling and linear buckling approaches in conjunction with von Kármán and Green-Lagrange stiffening. The results show that the IGA-TSDT solutions with Green-Lagrange stiffening are lower and closer to ANSYS solutions [1] than the solutions obtain using von Kármán stiffening. It is seen that the linear buckling approach predicts lower buckling load compared with the predictions using pre-buckling approach for plates with free boundary edges, explaining the lower strength exhibited by the structures. Particularly for CCCC, FCCC, FCFC, SCCC, and SCSC boundary conditions, the pre-buckling approach gives unrealistic results (as in this condition no buckling can occur) which can be confirmed from linear buckling approach which accounts for the clamped boundary conditions in linear static analysis.

4.3.4. *Effect of aspect ratio a/b*

This problem investigates the effect of aspect ratio a/b on the buckling strength of rectangular laminated composite plates using IGA-TSDT model. Six simply supported (SSSS) rectangular cross-ply laminated plates – (0°/90°/0°), (90°/0°/90°), (0°/90°/90°/0°), (90°/0°/0°/90°), (0°/90°), and $(0°/90°)_5$ – are considered in the parametric study. The lamainted plate is made of an MM2 material and is subjected to uniform uniaxial loads. Figs. 3, 4 and 5 show the variation of normalized buckling load $\bar{P}$ with respect to aspect ratio a/b for both moderately thick ($a/h = 10$) and thin ($a/h = 100$) plates. A comparison is also made between pre-buckling and linear buckling approaches.

It is observed that solutions obtained using linear buckling approach show a linearly varying stiffer response for increasing aspect ratio a/b unlike the response via pre-buckling approach. This behavior may be attributed to the non-uniform stress distribution caused by the clamped condition at the four corners. A similar behavior is also observed by Nima et al. [32] in their study using linear buckling approach for slightly different inplane constraints. Further, a noticeable difference is observed between solutions using Green-Lagrange and von Kármán stiffening for moderately thick plate $a/h = 10$; the Green-Lagrange stiffening underestimate the values of normalized buckling loads $\bar{P}$, supporting the usage of Green-Lagrange nonlinearity.

Table 2
Normalized buckling load $\bar{P}$ of simply supported (SSSS) square laminated plates under uniform uniaxial loads.

Lamination	a/h	von Kármán nonlinearity						Green-Lagrange nonlinearity				FEA	
		UTSDT[a]	UTSDT[b]	UTSDT[c]	TSDT[a]	TSDT[b]	TSDT[c]	UTSDT[b]	UTSDT[c]	TSDT[b]	TSDT[c]	ANSYS[b] [1]	ANSYS[c] [1]
(0°/90°/0°)	6	8.6752	8.6796	8.9878	8.7322	8.7323	9.0234	8.4921	8.8235	8.5071	8.8104	7.8242	8.0819
	8	11.6886	11.6921	12.0962	11.7775	11.7776	12.1707	11.5062	11.9282	11.5618	11.9646	10.7960	11.1549
	10	14.1201	14.1235	14.6050	14.2205	14.2207	14.6958	13.9511	14.4461	14.0249	14.5072	13.2670	13.7100
	20	20.0338	20.1373	20.7087	20.0987	20.0988	20.7716	19.9459	20.6212	20.0008	20.6754	19.5820	20.2376
	50	22.8554	22.8574	23.6219	22.8698	22.8700	23.6362	22.8372	23.6021	22.8492	23.6156	22.7590	23.5212
	100	23.3314	23.3323	24.1135	23.3352	23.3354	24.1173	23.3269	24.1082	23.3299	24.1119	23.3060	24.0870
$(0°/90°)_s$	6	8.7304	8.7395	9.0604	8.8022	8.8024	9.0379	8.5336	8.9262	8.5731	8.8561	N/A	7.4898
	8	11.6830	11.6897	12.2621	11.7842	11.7843	12.3273	11.4814	12.0766	11.5535	12.1049	11.1820	11.6946
	10	14.0650	14.0714	14.7449	14.1760	14.1761	14.8307	13.8752	14.5656	13.9608	14.6216	13.6050	14.2320
	20	19.9516	19.9584	20.8857	20.0226	20.0227	20.9503	19.8509	20.7826	19.9092	20.8377	19.7190	20.6320
	50	22.8337	22.8375	23.8945	22.8496	22.8498	23.9096	22.8133	23.8708	22.8251	23.8849	22.7850	23.8412
	100	23.3256	23.3271	24.4082	23.3298	23.3299	24.4123	23.3206	24.4019	23.3234	24.4058	23.3130	24.3940
(0°/90°)	6	6.7291	6.7834	7.1908	6.8253	6.8859	7.3118	6.5418	6.9808	6.6455	7.1016	6.5180	6.9150
	8	7.7189	7.7531	8.1834	7.7854	7.8237	8.2651	7.5377	7.9923	7.6085	8.0750	7.5510	7.9744
	10	8.2841	8.3078	8.7446	8.3315	8.3582	8.8022	8.1318	8.5874	8.1821	8.6460	8.1561	8.5882
	20	9.1819	9.1949	9.6318	9.1958	9.2100	9.6484	9.1312	9.5744	9.1461	9.5914	9.1480	9.5824
	50	9.4696	9.4818	9.9165	9.4719	9.4845	9.9194	9.4704	9.9062	9.4730	9.9091	9.4740	9.9081
	100	9.5122	9.5244	9.9589	9.5128	9.5251	9.9597	9.5215	9.9563	9.5222	9.9571	9.5224	9.9567
$(0°/90°)_2$	6	9.6194	8.8609	9.0387	10.1001	9.5781	9.7730	8.7820	8.9791	9.4765	9.6842	6.5897	6.6517
	8	12.4168	12.4230	13.0103	12.8711	12.8831	13.4944	12.2814	12.8834	12.7247	13.3438	10.4910	10.7059
	10	14.3682	14.3728	15.0519	14.7580	14.7678	15.4651	14.2334	14.9238	14.6138	15.3184	12.9860	13.6090
	20	18.2103	18.2118	19.0628	18.3663	18.3714	19.2274	18.1398	18.9951	18.2950	19.1547	17.6200	18.4480
	50	19.6923	19.6944	20.6083	19.7214	19.7248	20.6391	19.6795	20.5943	19.7094	20.6245	19.5810	20.4900
	100	19.9243	19.9268	20.8503	19.9317	19.9347	20.8582	19.9230	20.8466	19.9307	20.8544	19.8980	20.8200

[a] Denotes closed form solutions (CFS) using Navier approach.
[b] and [c] denote results using pre-buckling and linear buckling approaches, respectively.

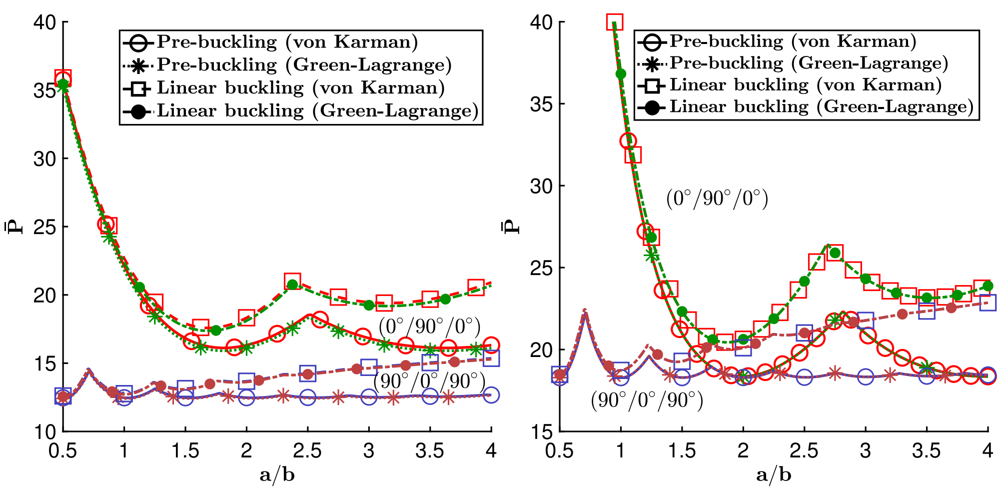

(a) $a/h = 10$. **(b)** $a/h = 100$.

Fig. 3. Effect of aspect ratio a/b on normalized buckling load $\bar{P} = Pb^2/E_2h^3$ of simply supported (SSSS) cross-ply (0°/90°/0°) and (90°/0°/90°) laminated plates under uniform uniaxial loads.

4.3.5. Effect of fiber orientation θ

An attempt is made here to study the influence of fiber orientation θ on the buckling characteristics of simply supported (SSSS) angle-ply laminated plates subjected to uniform uniaxial loads using IGA-TSDT model. Two laminates with material properties MM2 and stacking sequence $(\theta/-\theta)$ and $(\theta/-\theta)_5$ are considered. Fig. 6 shows the variation of the normalized buckling loads $\bar{P} = Pb^2/E_2h^3$ with ply orientation θ for plates with $a/h = 10$ and 100. Using the pre-buckling approach, the maximum buckling strength is observed at a ply orientation $\theta = 36°$ for $a/h = 10$ and $\theta = 40°$ for $a/h = 100$. The linear buckling approach, however, yields ply orientation $\theta = 50°$ for both thick ($a/h = 10$) and thin ($a/h = 100$) laminates. Further, a noticeable difference is also observed among solutions using Green-Lagrange and von Kármán stiffening which highlights the importance of including Green-Lagrange nonlinearity in the stress stiffening.
The complex variation of the normalized buckling strength $\bar{P}$ with ply orientation θ could be due to the presence of bending-twist coupling.

4.4. Nonlinear buckling analysis

Hereinafter, nonlinear methodologies are used to analyze the buckling behavior of laminated composite plates. The major feature of nonlinear approaches is that they provide complete information such as accurate buckling strength, unscaled displacement modes, and solution path, whereas

Table 3
Critical buckling load $\bar{P} = Pb^2/E_2h^3$ of simply supported (SSSS) square laminated plates with $a/h = 10$.

Lamination	E_1/E_2	von Kármán nonlinearity								Green-Lagrange nonlinearity						FEA	
		UTSDT[a]	UTSDT[b]	UTSDT[c]	UTSDT[d]	TSDT[a]	TSDT[b]	TSDT[c]	TSDT[d]	UTSDT[b]	UTSDT[c]	UTSDT[d]	TSDT[b]	TSDT[c]	TSDT[d]	ANSYS[c] [1]	ANSYS[d] [1]
$(0°/90°/0°)$	3	5.3896	5.3896	5.3966	6.7938	5.3898	5.3899	5.3899	6.7905	5.3121	5.2994	6.6752	5.3124	5.2897	6.6624	5.3878	6.7875
	10	9.8319	9.8319	9.8406	10.7867	9.8325	9.8326	9.8326	10.7779	9.7041	9.6736	10.6190	9.7047	9.6534	10.5898	9.8174	10.7610
	20	14.8882	14.8882	14.8943	15.6503	14.8896	14.8897	14.8897	15.6371	14.7154	14.6711	15.4378	14.7169	14.6436	15.3933	14.8390	15.5830
	30	18.8750	18.8750	18.8789	19.5296	18.8776	18.8778	18.8778	19.5136	18.6744	18.6228	19.2902	18.6772	18.5905	19.2349	18.7780	19.4093
	40	22.1164	22.1164	22.1189	22.6967	22.1207	22.1209	22.1209	22.6793	21.8973	21.8419	22.4400	21.9020	21.8063	22.3771	21.9600	22.5136
$(0°/90°)_s$	3	5.3932	5.3932	5.4037	7.2406	5.3933	5.3933	5.3933	7.2335	5.3158	5.2955	7.0948	5.3159	5.2831	7.0766	5.3905	7.2291
	10	9.9392	9.9392	9.9550	11.3014	9.9406	9.9406	9.9406	11.2820	9.8110	9.7551	11.0927	9.8125	9.7304	11.0503	9.9108	11.2470
	20	15.2900	15.2900	15.3017	16.3937	15.2984	15.2985	15.2985	16.3700	15.1167	15.0278	16.1296	15.1253	15.0041	16.0718	15.2080	16.2720
	30	19.6537	19.6537	19.6606	20.6128	19.6744	19.6745	19.6745	20.5933	19.4538	19.3445	20.3162	19.4749	19.3301	20.2546	19.5060	20.4150
	40	23.3026	23.3026	23.3059	24.1626	23.3400	23.3403	23.3403	24.1531	23.0866	22.9648	23.8468	23.1247	22.9651	23.7895	23.0780	23.8800
$(0°/90°)_1$	3	4.7748	4.7748	4.7869	6.4097	4.7749	4.7749	4.7884	6.4108	4.6880	4.6944	6.2920	4.6881	4.6940	6.2878	4.7818	6.3992
	10	6.2585	6.2586	6.2789	7.1461	6.2721	6.2722	6.2949	7.1631	6.1216	6.1287	7.0016	6.1352	6.1406	7.01341	6.2173	7.0767
	20	8.0439	8.0439	8.0645	8.6703	8.1151	8.1152	8.1379	8.7490	7.8640	7.8714	8.4954	7.9346	7.9398	8.5692	7.8903	8.4911
	30	9.7004	9.7004	9.7225	10.2307	9.8695	9.8697	9.8938	10.4115	9.4862	9.4977	10.0297	9.6536	9.6629	10.2053	9.4128	9.9182
	40	11.2604	11.2604	11.2850	11.7420	11.5625	11.5328	11.5896	12.0603	11.0169	11.0348	11.5190	11.3161	11.3320	11.8313	10.8236	11.2790
$(0°/90°)_5$	3	5.3875	5.3875	5.3876	7.2179	5.3882	5.3882	5.3887	7.2190	5.3093	5.3113	7.1185	5.3099	5.3102	7.1131	5.3823	7.2097
	10	10.0443	10.0443	10.0442	11.4007	10.0557	10.0558	10.0568	11.4140	9.9118	9.9204	11.2742	9.9232	9.9238	11.2737	10.0165	11.3682
	20	15.8699	15.8699	15.8701	16.9849	15.9141	15.9143	15.9156	17.0325	15.6881	15.7065	16.8271	15.7322	15.7336	16.8519	15.7995	16.9088
	30	20.8961	20.8961	20.8965	21.8762	20.9864	20.9865	20.9882	21.9711	20.6864	20.7137	21.7027	20.7765	20.7790	21.7671	20.7747	21.7484
	40	25.2777	25.2777	25.2785	26.1630	25.4225	25.4227	25.4246	26.3133	25.0536	25.0885	25.9839	25.1982	25.2018	26.0974	25.0998	25.9779

[a] Denotes closed form solutions (CFS) for assumed uniform stress distribution using Navier approach.
[b], [c], and [d] denote solutions using assumed stress, pre-buckling, and linear buckling approaches, respectively.

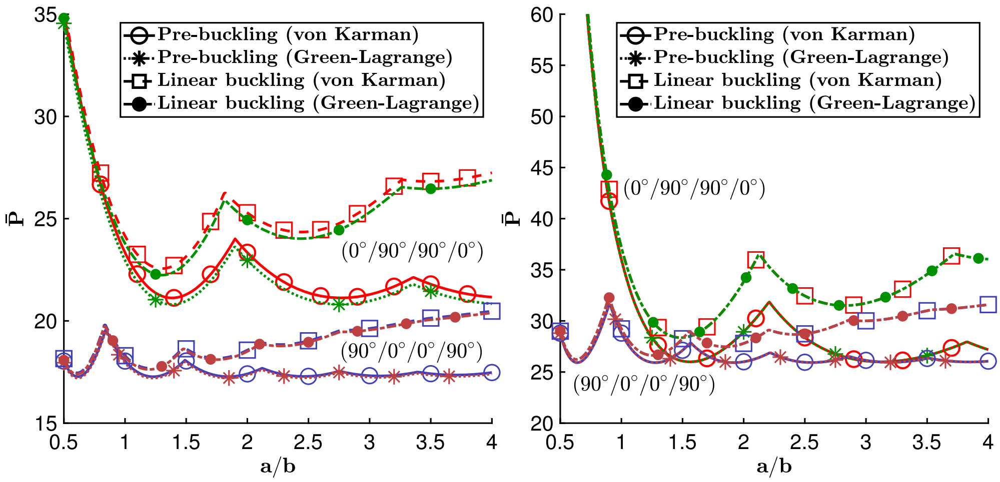

(a) $a/h = 10$. **(b)** $a/h = 100$.

Fig. 4. Effect of aspect ratio a/b on normalized buckling load $\bar{P} = Pb^2/E_2h^3$ of simply supported (SSSS) cross-ply $(0°/90°/90°/0°)$ and $(90°/0°/0°/90°)$ laminated plates under uniform uniaxial loads.

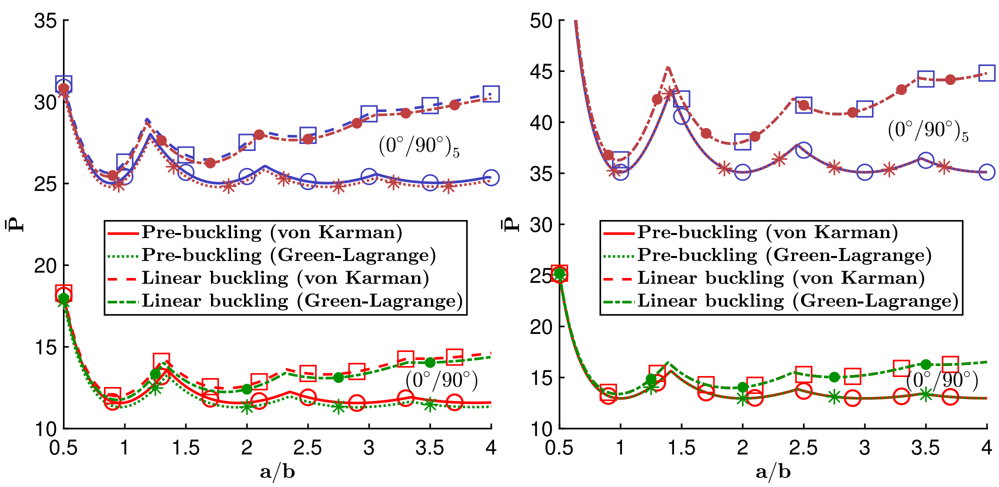

(a) $a/h = 10$. **(b)** $a/h = 100$.

Fig. 5. Effect of aspect ratio a/b on normalized buckling load $\bar{P} = Pb^2/E_2h^3$ of simply supported (SSSS) cross-ply $(0°/90°)$ and $(0°/90°)_5$ laminated plates under constant uniaxial loads.

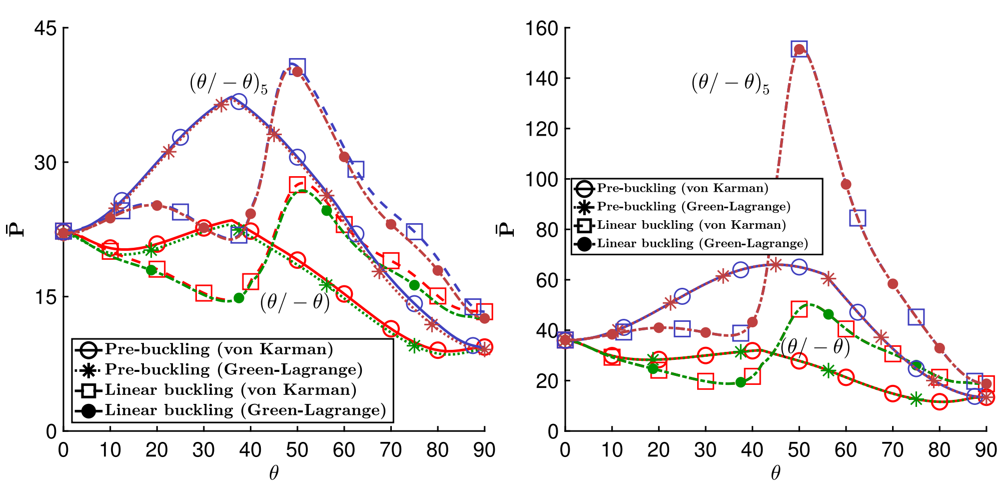

(a) $a/h = 10$. **(b)** $a/h = 100$.

Fig. 6. Effect of fiber orientation θ on normalized buckling load $\bar{P} = Pb^2/E_2h^3$ of simply supported (SSSS) angle-ply $(\theta/-\theta)$ and $(\theta/-\theta)_5$ laminated plates under uniform uniaxial loads.

Table 4
Normalized buckling load $\bar{P} = Pb^2/E_2h^3$ of square laminated $(0°/90°)_s$ plate subjected to uniaxial and biaxial compression with $b/h = 10$.

Boundary conditions	Approach	Uniform		Parabolic		Sinusoidal		Inverse sinusoidal		Triangular		Inverse triangular	
		Case-1	Case-2	Case-1	Case-2	Case-1	Case-2	Case-1	Case-2	Case-1	Case-2	Case-1	Case-2
CCCC	pre-buckling[a]	41.6973	21.4829	46.8442	24.2674	47.6980	24.7025	121.4590	73.8620	56.2032	29.0633	94.1738	55.9165
	pre-buckling[b]	41.2359	21.2937	46.3300	24.0594	47.1748	24.4919	111.6920	72.8925	55.5853	28.8212	90.5804	55.2596
	ANSYS [1]	39.5000	19.3110	44.5770	22.1470	45.3280	22.5690	53.7940	34.3760	48.9860	26.5810	50.6890	32.2850
FCCC	pre-buckling[a]	34.0080	10.4058	45.3225	12.4529	46.3388	12.7231	55.4820	38.3232	55.0738	15.1009	48.0442	26.9067
	pre-buckling[b]	33.6670	10.2806	44.8281	12.3602	45.8245	12.6326	54.1180	36.8935	54.4357	15.0034	47.0249	26.2669
	ANSYS [1]	33.3710	9.6578	43.1980	11.6160	44.0560	11.8760	49.8770	11.3490	48.9860	14.0910	46.7360	23.4480
	linear buckling[a]	-	11.9030	-	13.3045	-	13.5518	-	48.9515	-	18.9897	-	33.8872
	linear buckling[b]	-	11.8727	-	13.2690	-	13.5153	-	48.6484	-	15.9444	-	33.7578
	ANSYS [1]	-	10.9050	-	12.3210	-	12.5600	-	32.4470	-	14.8140	-	27.8020
CCCF	pre-buckling[a]	18.8781	10.9193	20.5442	16.4776	20.8933	17.1713	75.2280	28.5160	24.5486	21.2740	54.6552	21.4581
	pre-buckling[b]	18.7023	10.8424	20.3744	16.3605	20.7227	17.0487	72.4167	28.3126	24.3554	21.1187	53.9993	21.3011
	ANSYS [1]	17.8320	10.1600	19.5790	15.3460	19.9240	16.0010	51.5970	21.3500	23.4050	19.8890	46.9260	19.9020
	linear buckling[a]	18.7491	18.7491	20.7610	20.7610	21.1198	21.1198	72.8009	72.8009	24.8034	24.8034	53.2586	53.2586
	linear buckling[b]	18.5798	18.5798	20.5920	20.5920	20.9500	20.9500	71.5540	71.5540	24.6111	24.6111	52.6565	52.6565
	ANSYS [1]	17.7350	17.7350	19.7820	19.7820	20.1370	20.1370	51.3820	51.3820	23.6430	23.6430	46.2670	46.2670
CFFC	pre-buckling[a]	7.8602	3.6063	12.5901	6.4091	13.1451	6.7696	15.1488	6.6856	16.4865	8.7284	12.4543	5.5207
	pre-buckling[b]	7.8058	3.5887	12.5128	6.3810	13.0650	6.7402	15.0245	6.6486	16.3877	8.6918	12.3571	5.4912
	ANSYS [1]	7.8037	3.5422	12.3980	6.2493	12.9270	6.5909	15.0850	6.5952	16.1470	8.4639	12.4070	5.4445
	linear buckling[a]	7.8597	3.6051	12.5210	6.3567	13.0713	6.7141	15.3968	6.7836	16.3931	8.6650	12.5980	5.5787
	linear buckling[b]	7.8054	3.5875	12.4446	6.3277	12.9921	6.6838	15.2720	6.7468	16.2957	8.6266	12.5007	5.5494
	ANSYS [1]	7.8035	3.5412	12.3380	6.2023	12.8640	6.5417	15.3340	6.6906	16.0690	8.4088	12.5500	5.5011
CFCF	pre-buckling[a]	12.6742	7.0443	13.7597	10.2810	14.0115	10.6947	70.7270	20.2680	16.5922	13.2719	44.1188	14.7657
	pre-buckling[b]	12.5900	6.9956	13.6884	10.2181	13.9411	10.3605	69.6954	20.0934	16.5161	13.1976	43.6367	14.6421
	ANSYS [1]	11.2100	6.3253	12.3200	9.2132	12.5590	9.5824	51.3750	18.2700	14.8940	11.8890	37.5650	13.2990
	linear buckling[a]	12.5366	12.5366	13.9429	13.9429	14.2049	14.2049	67.1682	67.1682	16.8225	16.8225	41.8124	41.8124
	linear buckling[b]	12.4553	12.4553	13.8709	13.8709	14.1336	14.1336	66.2743	66.2743	16.7456	16.7456	41.3778	41.3778
	ANSYS [1]	11.1030	11.1030	12.4700	12.4700	12.7180	12.7180	50.7760	50.7760	15.0870	15.0870	35.9280	35.9280
FCFC	pre-buckling[a]	41.3778	9.6461	42.7937	11.4692	43.8569	11.7186	53.0943	37.8628	52.5861	13.9298	45.7794	26.0615
	pre-buckling[b]	33.1168	9.5280	42.3675	11.3817	43.4111	11.6333	51.9142	36.4551	52.0227	13.8385	44.8368	25.4416
	ANSYS [1]	32.6720	9.0288	41.5360	10.8070	42.4750	11.0500	49.8770	29.5980	48.9860	13.1370	44.8710	22.8800
	linear buckling[a]	-	11.0167	-	12.4296	-	12.6661	-	45.3885	-	14.9805	-	32.7106
	linear buckling[b]	-	11.0818	-	12.4013	-	12.6371	-	48.1143	-	14.9452	-	32.5987
	ANSYS [1]	-	10.2510	-	11.6080	-	11.8400	-	32.3810	-	14.0040	-	27.1790
CFFF	pre-buckling[a]	1.1517	0.8789	1.9603	1.6247	2.0739	1.7327	2.4738	1.7167	2.7002	2.2979	1.9463	1.3849
	pre-buckling[b]	1.1470	0.8753	1.9510	1.6165	2.0639	1.7238	2.4664	1.7116	2.6868	2.2857	1.9398	1.3804
	ANSYS [1]	1.1055	0.8494	1.8699	1.5579	1.9758	1.6590	2.3953	1.6733	2.5645	2.1925	1.8819	1.3479
	linear buckling[a]	1.1515	0.8788	1.9639	1.6015	2.0779	1.7056	2.4673	1.7414	2.7058	2.2556	1.9428	1.3994
	linear buckling[b]	1.1467	0.8751	1.9545	1.5935	2.6786	1.6970	2.4599	1.7362	2.6924	2.2437	1.9363	1.3949
	ANSYS [1]	1.1053	0.84924	1.8731	1.5362	1.9794	1.6337	2.3892	1.6971	2.5697	2.1531	1.8786	1.3620
FFFC	pre-buckling[a]	6.2460	2.1727	8.9676	3.9822	9.3209	4.2389	12.9790	4.2058	11.6271	5.5906	10.9822	3.4098
	pre-buckling[b]	6.2296	2.1623	8.9412	3.9621	9.2931	4.2174	12.8274	4.1877	11.5915	5.5623	10.8436	3.3948
	ANSYS [1]	6.2409	2.1426	8.9648	3.9000	9.3139	4.1451	12.9710	4.1744	11.5920	5.4474	10.9690	3.3818
	linear buckling[a]	6.2460	2.1724	8.9625	3.9329	9.3145	4.1820	13.5085	4.2599	11.6156	5.5044	11.3225	3.4420
	linear buckling[b]	6.2296	2.1620	8.9364	3.9130	9.2870	4.1608	13.3472	4.2417	11.5803	5.4764	11.1771	3.4268
	ANSYS [1]	6.2409	2.1423	8.9609	3.8541	9.3088	4.0924	13.4910	4.2267	11.5820	5.3680	11.3040	3.4129

Case 1: uniaxial compression; Case2: biaxial compression.
[a] and [b] denotes IGA-TSDT solutions using von Kármán nonlinearity and Green-Lagrange nonlinearity, respectively.

linear eigenvalue buckling analysis gives scaled buckling modes. Two nonlinear approaches are used in this study, namely, nonlinear buckling approach and nonlinear eigenvalue approach. The former deals with the solution of nonlinear static problems using tangent based arc-length method and the latter is used for linear eigenvalue problems with augmented nonlinear stiffness. The solution methodology of the nonlinear eigenvalue approach comprises two steps. Firstly, linear buckling analysis is conducted using either pre-buckling approach or linear buckling approach. Then, nonlinear eigenvalue analysis is solved using direct iterative technique.

The present study also examines the influence of initial imperfection on the buckling characteristic of composite plate structures as imperfection in many physical structures is inherent. To switch from primary solution path to secondary solution path in nonlinear buckling analysis, a perturbation type simple path switching technique is utilized in conjunction with arc-length method. Because NURBS basis functions do not satisfy Kronecker delta property, a one-to-one mapping of imperfection to control points yields non-exact imperfection in the physical space. A scaling technique has been proposed to incorporate exact imperfection in the IGA framework as discussed in Section 3.2. The present study is limited to sinusoidal type imperfection, which is equivalent to the first buckling mode obtained from the linear buckling analysis.

4.4.1. Simply supported isotropic plate

To validate the nonlinear formulation, a result from Yamaky, as reported in Ref. [59], and Ganapati et al. [59] is replicated. For this, a simply supported (SSSS) isotropic ($E = 1$ GPa and $\nu = 0.3$) plate subjected to uniform uniaxial load is studied using IGA-TSDT for both nonlinear buckling and nonlinear eigenvalue approaches. For the nonlinear eigenvalue approach, an initial linear buckling analysis is conducted using pre-buckling/linear buckling approach, and then a nonlinear eigenvalue analysis is carried out using simply supported (SSSS) boundary conditions.

Table 5
Normalized buckling load $\bar{P} = Pb^2/E_2h^3$ of square laminated $(0^\circ/90^\circ)_s$ plate subjected to uniaxial and biaxial compression with $b/h = 10$.

Boundary conditions	Approach	Uniform		Parabolic		Sinusoidal		Inverse sinusoidal		Triangular		Inverse triangular	
		Case-1	Case-2	Case-1	Case-2	Case-1	Case-2	Case-1	Case-2	Case-1	Case-2	Case-1	Case-2
CCCS	pre-buckling[a]	36.8860	18.3363	41.7662	21.0602	42.5761	21.4901	117.9420	63.6947	50.4217	25.5265	92.2550	49.6448
	pre-buckling[b]	36.4270	18.1728	41.2882	20.8862	42.0932	21.3144	111.6390	62.9118	49.8644	25.3250	90.4499	49.0889
	ANSYS [1]	35.2060	17.1070	40.1670	19.7230	40.9710	20.1290	53.7930	34.3730	48.4950	23.8660	50.6890	32.2830
	linear buckling[a]	37.7309	37.7309	42.8905	42.8905	43.7883	43.7883	131.6420	131.6420	52.1361	52.1361	100.5190	100.5190
	linear buckling[b]	37.2774	37.2774	42.4106	42.4106	43.3025	43.3025	119.181	119.181	51.5711	51.5711	95.1530	95.1530
	ANSYS [1]	36.1060	36.1060	41.3660	41.3660	42.2570	42.2570	59.3260	59.3260	49.7090	49.7090	55.5920	55.5920
SCCC	pre-buckling[a]	39.7398	18.6859	45.8206	22.3245	46.7415	22.9062	107.2860	64.8927	55.3163	27.7425	85.6468	49.3556
	pre-buckling[b]	39.1686	18.5047	45.2677	22.1385	46.1807	22.7165	69.7783	63.4977	54.6536	27.5135	63.6191	48.4772
	ANSYS [1]	38.0310	17.2460	43.5100	20.7900	44.3100	21.3490	53.7920	34.3730	48.9860	25.8840	-	32.2830
	linear buckling[a]	-	24.3834	-	27.8858	-	28.4965	-	90.8411	-	34.0566	-	68.8426
	linear buckling[b]	-	24.2789	-	27.7649	-	28.3728	-	90.3538	-	33.9083	-	68.5264
	ANSYS [1]	-	21.8080	-	25.1590	-	25.7220	-	38.9980	-	30.7020	-	36.2750
CSSC	pre-buckling[a]	32.8623	15.7913	38.2093	18.8302	39.0617	19.3087	104.5980	54.9677	46.7067	23.3215	84.2056	41.7482
	pre-buckling[b]	32.3684	15.6384	37.7601	18.6842	38.6111	19.1614	69.7342	53.8115	46.1918	23.1498	63.5971	41.1094
	ANSYS [1]	31.9770	14.9620	37.2810	17.9980	38.1160	18.4690	53.7920	34.3710	45.4810	22.3090	50.6880	32.2810
	linear buckling[a]	34.6972	16.9085	40.0695	19.9396	40.9953	20.4643	118.0510	59.6192	49.1874	24.8354	92.7613	45.8859
	linear buckling[b]	34.2220	16.7621	39.6088	19.7895	40.5314	20.3120	84.7653	58.4739	48.6524	24.6551	74.8202	45.2054
	ANSYS [1]	33.7520	16.0400	39.1430	19.0740	40.0550	19.5890	59.3300	37.9240	47.9880	23.7790	55.5960	35.0600
CSCS	pre-buckling[a]	34.0608	15.3524	39.1457	17.7978	39.9715	18.1891	116.9190	63.2870	47.6706	21.7379	92.1474	47.2360
	pre-buckling[b]	33.6275	15.2178	38.7082	17.6559	39.5319	18.0458	111.5990	62.5123	47.1717	21.5732	90.3145	46.6933
	ANSYS [1]	31.9590	14.5780	37.0160	16.9310	37.8310	17.3040	53.7930	34.3730	45.1600	20.6380	50.6890	32.2830
	linear buckling[a]	33.8958	33.8958	38.3756	38.3756	39.1835	39.1835	127.0500	127.0500	46.7734	46.7734	97.1087	97.1087
	linear buckling[b]	33.4768	33.4768	37.9544	37.9544	38.7599	38.7599	117.0830	117.0830	46.2912	46.2912	93.5461	93.5461
	ANSYS [1]	31.8350	31.8350	36.3490	36.3490	37.1450	37.1450	59.1710	59.1710	44.3690	44.3690	55.5280	55.5280
SCSC	pre-buckling[a]	37.0756	17.8356	43.3646	21.3779	44.3310	21.9486	107.1430	64.8890	52.8907	26.6573	85.4887	49.1958
	pre-buckling[b]	36.5053	17.6571	42.8498	21.1892	43.8122	21.7555	69.7780	63.4949	52.2840	26.4202	63.6176	48.4418
	ANSYS [1]	36.1540	16.5050	42.0130	19.9440	42.8720	20.4890	53.7920	34.3730	48.9860	24.8810	50.6880	32.2830
	linear buckling[a]	-	22.8455	-	25.9593	-	26.5163	-	88.9714	-	31.6865	-	67.5328
	linear buckling[b]	-	22.7536	-	25.8541	-	26.4088	-	88.5474	-	31.5578	-	67.2597
	ANSYS [1]	-	20.8140	-	23.9440	-	24.4860	-	38.7690	-	29.3030	-	36.0650
SSSC	pre-buckling[a]	29.4151	15.6159	34.5833	18.3877	35.4122	18.8324	104.5380	54.9016	42.5917	22.6740	82.8646	40.7917
	pre-buckling[b]	28.9475	15.4715	34.1796	18.2585	35.0089	18.7029	69.7339	53.7488	42.1333	22.5252	63.5957	40.1973
	ANSYS [1]	29.0120	14.8180	34.1960	17.9080	35.0160	18.3420	53.7920	34.3700	42.0230	22.0330	50.6880	32.2810
	linear buckling[a]	31.2688	16.4717	36.4824	19.1272	37.3831	19.5941	117.9420	59.1051	45.1067	23.6415	91.2600	44.4986
	linear buckling[b]	30.8262	16.3400	36.0655	19.9988	36.9642	19.4646	84.7638	58.0193	44.6246	23.4905	74.8155	43.8919
	ANSYS [1]	30.8340	15.5920	36.0890	18.5330	36.9820	19.0320	59.3450	37.9840	44.5400	22.9750	55.6080	35.2320
CSSS	pre-buckling[a]	27.7543	12.7377	32.5688	15.1256	33.3403	15.5091	103.9210	54.8859	40.0886	18.7474	83.3406	36.8543
	pre-buckling[b]	27.3326	12.6180	32.1903	15.0126	32.9620	15.3955	69.7155	53.7384	39.6608	18.6161	63.5838	36.3363
	ANSYS [1]	26.8720	12.3600	31.6460	14.7460	32.4070	15.1240	53.7920	34.3700	38.9360	18.2610	50.6880	32.2810
	linear buckling[a]	28.7406	13.4173	32.9805	15.6992	33.7370	16.0999	115.3350	59.0894	40.5293	19.4985	90.4799	40.1115
	linear buckling[b]	28.3254	13.2973	32.6003	15.5827	33.3567	15.9824	83.8437	57.9606	40.0986	19.3617	73.9317	39.5678
	ANSYS [1]	27.8050	13.0210	32.0570	15.3210	32.8030	15.7170	59.1740	38.1960	39.3740	19.0170	55.5310	35.4040

Case 1: uniaxial compression; Case2: biaxial compression.
[a] and [b] denote IGA-TSDT solutions using von Kármán nonlinearity and Green-Lagrange nonlinearity, respectively.

Fig. 7 shows the plots of the obtained IGA-TSDT solutions with ANSYS solutions [1], FSDT solutions by Ganapathi et al. [59], and CLPT solutions by Yamaky [59] for plates with $a/h = 10$ and 100. Here, the reference solutions are calculated using the nonlinear eigenvalue approach in conjunction with pre-buckling analysis. In Fig. 7, the present solution using the nonlinear eigenvalue approach and nonlinear buckling approach are labeled as "NL Eigenvalue" and "NL Buckling", respectively, where stress stiffening is indicated in parenthesis. In addition, nonlinear eigenvalue solutions are labeled as "Prebuckling" and" L Buckling" for pre-buckling and linear buckling approaches used in the linear static analysis, respectively.

It is observed that the present post-buckling response using nonlinear eigenvalue approach with pre-buckling approach is in good agreement with FSDT solution of Ganapathi et al. [59]. The response from the nonlinear eigenvalue approach using linear buckling approach is found to be in close agreement with that of the nonlinear buckling approach, confirming the need for consistent boundary conditions in the linear buckling analysis. Further, a substantial difference is observed between solutions of nonlinear eigenvalue approach with pre-buckling approach and nonlinear buckling approach for moderately thick plate $a/h = 10$. The same is also observed between results using nonlinear buckling approaches with von Kármán and Green-Lagrange stress stiffening, highlighting the significance of Green-Lagrange nonlinearity for safer and reliable design.

It is obvious from Fig. 7 that the nonlinear buckling approach is more reliable and accurate than the nonlinear eigenvalue approach; solving the whole problem with a single set of boundary conditions better captures the physical situation. The nonlinear eigenvalue approach with linear buckling approach on the other hand gives accurate post-buckling response up to $w_{\max}/h = 0.9$, giving a computational advantage over the computational intensive nonlinear buckling approach. The nonlinear eigenvalue approach also gives questionable predictions after $w_{\max}/h = 0.9$ and displays structural snapping.

4.4.2. *Symmetric cross-ply laminated plate with and without sinusoidal imperfection*

The numerical simulations here examine the effect of geometric imperfections on the post-buckling characteristics of symmetric cross-ply laminated composite plates using two simply supported (SSSS) square laminated $(0^\circ/90^\circ/90^\circ/0^\circ)$ plates with side-to-thickness ratio $b/h = 10$ and 100.

Table 6
Normalized buckling load $\bar{P} = Pb^2/E_2h^3$ of square laminated $(0°/90°)_s$ plate subjected to uniaxial and biaxial compression with $b/h = 10$.

Boundary conditions	Approach	Uniform		Parabolic		Sinusoidal		Inverse sinusoidal		Triangular		Inverse triangular	
		Case-1	Case-2	Case-1	Case-2	Case-1	Case-2	Case-1	Case-2	Case-1	Case-2	Case-1	Case-2
SSSS	pre-buckling[a]	23.3402	11.6701	27.5833	13.8129	28.2694	14.1618	103.892	54.7352	34.1283	17.1226	69.9056	35.4676
	pre-buckling[b]	22.9650	11.5623	27.2636	13.7176	27.9509	14.0665	69.7151	53.6063	33.7692	17.0142	63.5824	34.9069
	ANSYS [1]	23.0780	11.5390	27.3580	13.7000	28.0440	14.0480	53.7920	34.3698	33.8130	16.9610	50.6880	32.2810
	linear buckling[a]	24.1530	12.0770	27.9517	13.9976	28.6267	14.3406	115.224	58.5872	34.5285	17.3221	76.2311	38.2528
	linear buckling[b]	23.7891	11.9737	27.6310	13.9036	28.3068	14.2465	83.8424	57.5311	34.1671	17.2145	73.8966	37.6975
	ANSYS [1]	23.8800	11.9410	27.7370	13.8900	28.4110	14.2320	59.1840	38.2160	34.2220	17.1650	55.5340	35.5140
SSSF	pre-buckling[a]	11.9737	3.6521	13.5072	5.4843	13.8048	5.7363	60.4175	9.8455	16.5435	7.2678	37.9976	7.2412
	pre-buckling[b]	11.9698	3.6355	11.9698	5.4642	13.7175	5.7158	51.7221	9.7828	16.4487	7.2434	37.0857	7.1991
	ANSYS [1]	11.7920	3.5335	13.2170	5.3144	13.5090	5.5571	51.1500	9.5082	16.1610	7.0317	36.3010	7.0076
	linear buckling[a]	11.5763	3.6060	13.3687	5.4560	13.6793	5.7086	53.4616	9.5757	16.4225	7.2362	34.1253	7.0844
	linear buckling[b]	11.4737	3.5915	13.2848	5.4372	13.5965	5.6893	52.3070	9.5264	16.3316	7.2131	33.5681	7.0500
	ANSYS [1]	11.2790	3.4890	13.0690	5.2856	13.3750	5.5288	48.0160	9.2539	16.0320	6.9995	32.7300	6.8581
FSSS	pre-buckling[a]	18.1243	7.3651	25.6263	9.2487	26.4558	9.4923	33.6797	24.4071	32.4338	11.4351	28.3037	17.4712
	pre-buckling[b]	17.9572	7.2792	25.4078	9.1777	26.2304	9.4226	33.1850	23.9142	32.1601	11.3597	27.9123	17.1659
	ANSYS [1]	18.0560	7.1925	25.5110	9.0214	26.3300	9.2577	33.6040	23.6860	32.2170	11.1280	28.2290	17.0660
	linear buckling[a]	18.0570	7.2827	25.7666	9.2291	26.6087	9.4751	33.5378	23.3225	32.6444	11.4203	28.1371	16.8842
	linear buckling[b]	17.8904	7.1968	25.5495	9.1573	26.3844	9.4045	33.0449	22.8580	32.3710	11.3438	27.7476	16.5924
	ANSYS [1]	17.9890	7.1114	25.6540	8.9992	26.4860	9.2379	33.4590	22.6620	32.4310	11.1110	28.0620	16.5030
SFSF	pre-buckling[a]	5.0633	2.8243	5.7360	4.2050	5.8721	4.3908	32.5054	7.8203	7.0833	5.5280	16.9200	5.7182
	pre-buckling[b]	5.0133	2.8031	5.7048	4.1809	5.7048	4.3664	31.3390	7.7327	7.0519	5.4998	16.5331	5.6604
	ANSYS [1]	4.8575	2.7107	5.5280	4.0403	5.6600	4.2177	30.1790	7.4864	6.8185	5.3033	16.0580	5.4867
	linear buckling[a]	4.9140	2.7784	5.7045	4.1725	5.8446	4.3584	28.0851	7.5780	7.0585	5.4900	15.5120	5.5734
	linear buckling[b]	4.8750	2.7605	5.6752	4.1504	5.8162	4.3360	27.4542	7.5107	7.0286	5.4640	15.2646	5.5274
	ANSYS [1]	4.7264	2.6666	5.4939	4.0078	5.6300	4.1854	26.2810	7.2590	6.7913	5.2656	14.7550	5.3494
FSFS	pre-buckling[a]	17.7566	7.1930	24.6760	8.7586	25.5199	8.9733	30.3485	22.4283	31.4453	10.7724	25.8567	16.3589
	pre-buckling[b]	17.6621	7.1065	24.5116	8.6909	25.3470	8.9069	29.8533	22.0578	31.2255	10.7010	25.4122	16.1186
	ANSYS [1]	17.6880	7.0174	24.5970	8.5591	25.4320	8.7700	30.3950	22.0130	31.2730	10.5130	25.8730	16.1170
	linear buckling[a]	17.7568	7.1424	24.7548	8.7466	25.6103	8.9628	30.6663	21.6143	31.5814	10.7639	26.0469	15.8700
	linear buckling[b]	17.6623	7.0555	24.5908	8.6782	25.4377	8.8958	30.1645	21.2589	31.3614	10.6916	25.5980	15.6381
	ANSYS [1]	17.6880	6.9680	24.6740	8.5459	25.5200	8.7584	30.7030	21.2180	31.4080	10.5030	26.0590	15.6360

Case-1: uniaxial compression; Case-2: biaxial compression.
[a] and [b] denote IGA-TSDT solutions using von Kármán nonlinearity and Green-Lagrange nonlinearity, respectively.

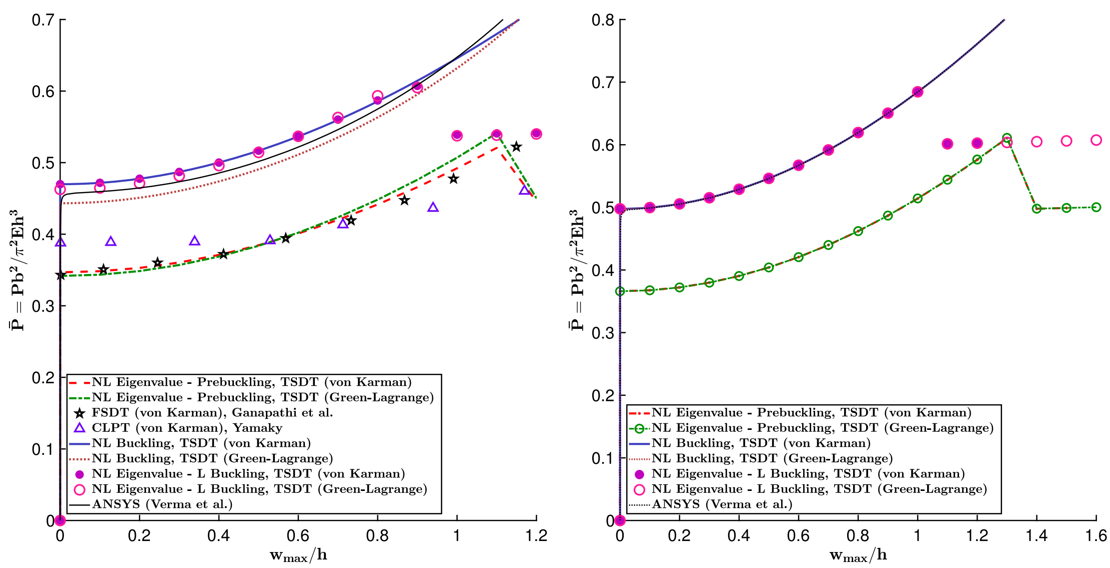

Fig. 7. Comparison of nonlinear eigenvalue and nonlinear buckling approaches for buckling and post-buckling analysis of simply supported (SSSS) isotropic plate under uniform uniaxial load with $a/h = 10$ and $a/h = 100$.

The plates, with MM1 material properties [58], are subjected to uniform uniaxial loads. Fig. 8 depicts plots of the load-deflection response of laminated composite plates using IGA-TSDT model with ANSYS solutions [1] for different magnitudes of imperfections, ranging from $w_0^* = 0$ (flat plate) to $w_0^*/h = 1\times10^{-2}$, 5×10^{-2}, and 10×10^{-2} for sinusoidal imperfection function $w^* = w_0^* sin(\pi x/a)\, sin(\pi y/b)$. Numerical results are obtained using both nonlinear buckling and nonlinear eigenvalue approaches in terms of normalized load parameter $\bar{P} = Pb^2/h^3E_2$ and normalized maximum deflection $\bar{w} = w_{max}/h$. It is plausible to posit that the imperfect plates do not exhibit bifurcation and they deflect with increase in the imperfection

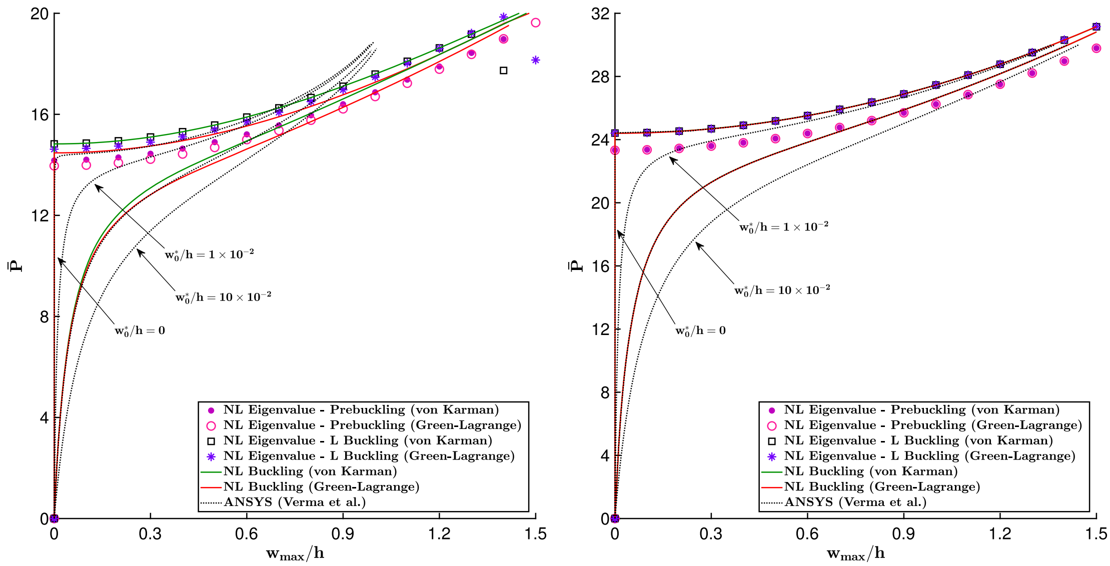

(a) $b/h = 10$. **(b)** $b/h = 100$.

Fig. 8. Buckling response of a simply supported (SSSS) square laminated (0°/90°/90°/0°) plate with and without imperfection under uniaxial loads.

amplitude w_0^*. A close agreement is also observed between the present IGA-TSDT solutions using nonlinear buckling approach and ANSYS solutions [1] for $w_0^*/h = 5\times10^{-2}$. Further, the normalized value of the initial buckling strength $\bar{P}$ of the thin ($a/h = 100$) plate using pre-buckling approach is calculated to be 23.3927 (von Kármán) and 23.3927 (Green-Lagrange) while with linear buckling approach, it is found to be 24.4712 (von Kármán) and 24.4646 (Green-Lagrange). Repeating the calculation for the moderately thick ($a/h = 10$) plate, the normalized value of the initial buckling strength $\bar{P}$ using pre-buckling approach is found to be 14.1967 (von Kármán) and 13.9812 (Green-Lagrange) while with linear buckling it is observed to be 14.848 (von Kármán) and 14.6393 (Green-Lagrange).

Fig. 8 also shows that the effect of stress stiffening is important for moderately thick plate structures because results obtained using Green-Lagrange nonlinearity are closer to ANSYS solutions [1] and are lower than the results obtained using von Kármán nonlinearity. A very close agreement is also found between the nonlinear buckling approach and nonlinear eigenvalue approach with linear buckling approach up to $w_{max}/h = 1.14$. Hence, nonlinear eigenvalue approach is an effective substitute of nonlinear buckling approach for symmetric cross-ply flat laminated plates up to $w_{max}/h = 1$. Further, the through-thickness variation of stresses for both moderately thick and thin plates is plotted along with ANSYS solutions [1] in Figs. 9 and 10, respectively, highlighting the importance of Green-Lagrange stiffening and HSDT models over FSDT model. It is observed that Figs. 8 and 9 do not exhibit any tertiary post-buckling response as seen in the Ref. [1]. This could be attributed to C^0 implementation of the FEM-TSDT in [1].

4.4.3. *Anti-symmetric cross-ply laminated plate*

Anti-symmetric cross-ply laminated composite plates have applications in reconfigurable antenna, lighting striker, morphing structures, and stiffened plates with omega stringers. This section presents a case study using square laminated plates for stacking sequence: (0°/90°), $(0°/90°)_2$, and $(0°/90°)_5$. But for the Young's modulus ratio which is set as $E_1/E_2 = 40$, the remaining parameters, such as boundary conditions, loading condition, geometric properties, and material properties, are identical to those used in the preceding section, Section 4.4.2. The same problem with $a/h = 100$ is studied by Giri and Simitses [57], and Prabhakara [56] using CLPT in conjunction with von Kármán nonlinearity. Fig. 11 depicts the plot of the load-deflection response of the anti-symmetric cross-ply laminated plates using both nonlinear eigenvalue and nonlinear buckling approaches for IGA-TSDT model along with ANSYS solutions [1]. The anti-symmetric cross-ply laminated plates do not exhibit bifurcation buckling due to the presence of bending-stretching coupling. The results predicted by both the nonlinear eigenvalue approach and the linear buckling approach are invalid because bifurcation is not observed. Therefore, nonlinear buckling approach must be used for a reliable and effective buckling analysis of general composite plates.

4.4.4. *Effect of aspect ratio a/b on nonlinear buckling response*

The effect of aspect ratio a/b on the post-buckling response of the laminated composite plates is now investigated as was done in the linear analysis, Section 4.3.4. A simply supported (SSSS) thin ($b/h = 100$) rectangular laminated (0°/90°/0°) plate is considered for a parametric study and the material properties of the constituents are MM2.

The plate is subjected to uniform uniaxial loads with magnitude P. Fig. 12 shows plots of the load-deflection curves of post-buckling characteristics of composite plates for different aspect ratios $a/b = 0.5, 1, 1.5, 2, 2.5, 3, 3.5, 4, 4.5,$ and 5. The present IGA-TSDT results, in terms of normalized load $\hat{P} = \bar{P}/\bar{P}_{critical}$ and normalized maximum deflection w_{max}/h, are obtained using nonlinear buckling and nonlinear eigenvalue approaches with linear buckling analysis in conjunction with von Kármán nonlinearity since the plate is thin $b/h = 100$. The initial buckling strength $\bar{P}_{critical} = P_{critical} b^2/E_2 h^3$ for different aspect ratios $a/b = 0.5, 1, 1.5, 2, 2.5, 3, 3.5, 4, 4.5,$ and 5 are 126.4560, 35.9256, 20.9794, 18.3582, 20.0377, 20.9908, 18.8983, 18.3621, 18.8374, and 19.4187, respectively. It is observed in Fig. 12 that the plate buckles with higher buckling modes with increasing aspect ratio. Further, the nonlinear eigenvalue approach accurately captures the post-buckling response up to $w_{max}/h = 0.8$. The mode shapes shown in Fig. 12 are for the nonlinear buckling approach.

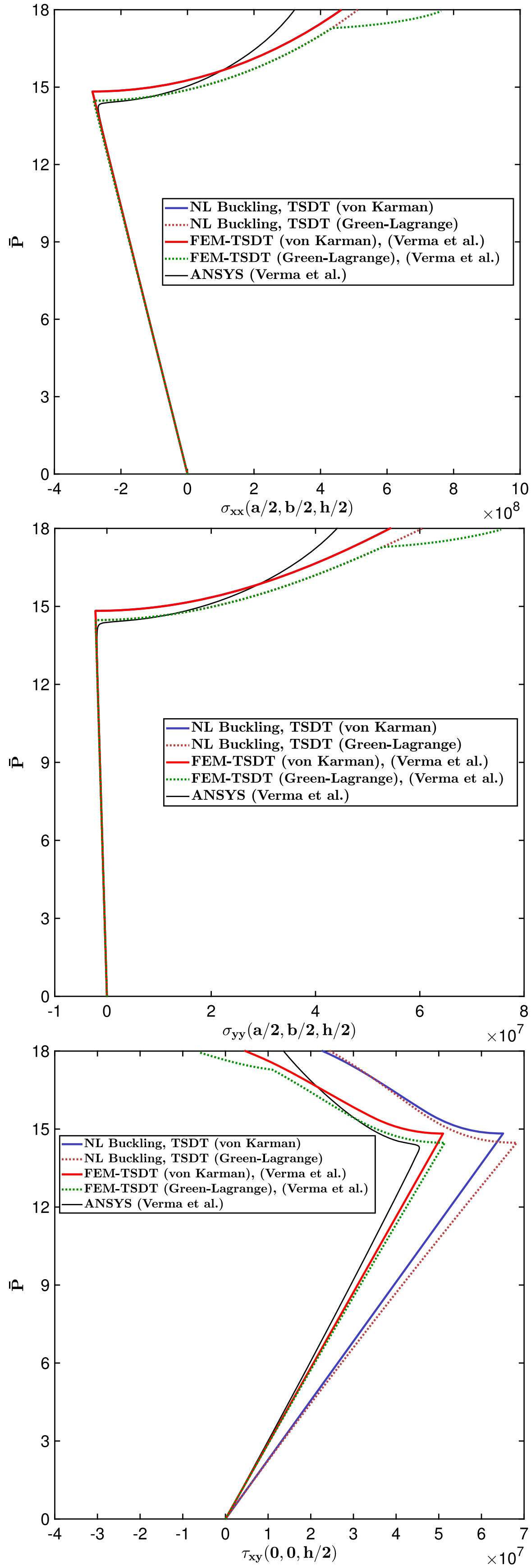

Fig. 9. Variation of stresses at critical points for buckling and post-buckling analysis of simply supported (SSSS) square symmetric laminated (0°/90°/90°/0°) plate under uniaxial load with $a/h = 10$.

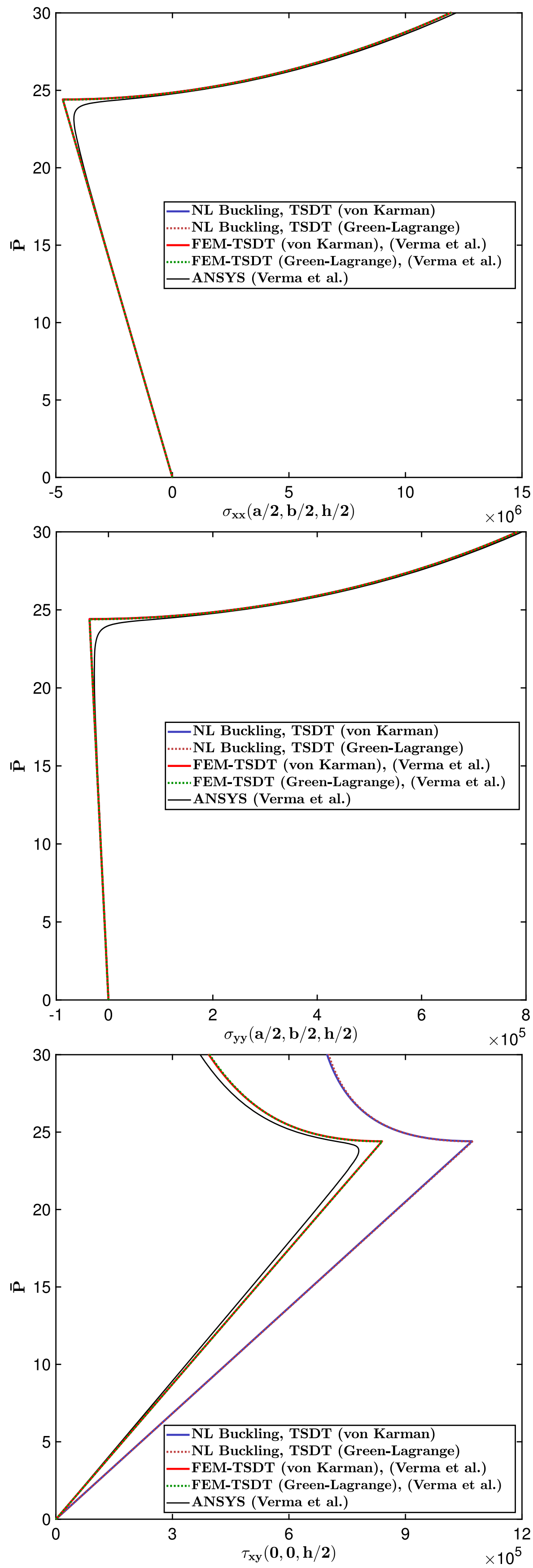

Fig. 10. Variation of stresses at critical points for buckling and post-buckling analysis of simply supported (SSSS) square symmetric laminated (0°/90°/90°/0°) plate under uniaxial load with $a/h = 100$.

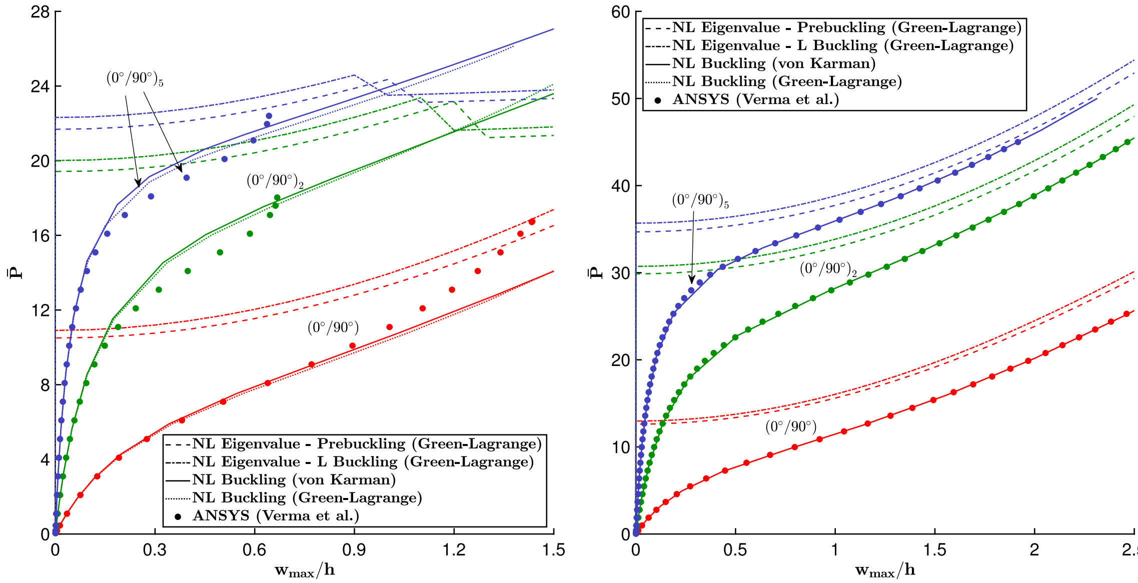

(a) $a/h = 10$. **(b)** $a/h = 100$.

Fig. 11. Nonlinear response of anti-symmetric cross-ply laminated plates under uniform uniaxial loads with different ply configurations $(0°/90°)$, $(0°/90°)_2$, and $(0°/90°)_5$ depicted in red, green, and blue colors, respectively. (For interpretation of the colors in the figure(s), the reader is referred to the web version of this article.)

4.4.5. Effect of boundary conditions on nonlinear buckling response

The simulation presented here is an investigation of the effect of different boundary conditions on the post-buckling response of the laminated composite plates as reported in Section 4.3.3. For this parametric study, a thin $(b/h = 100)$ square laminated $(0°/90°/90°/0°)$ composite plate is considered. The plate is subjected to a uniform uniaxial load with magnitude P.

The remaining parameters, such as material properties, normalized load $\hat{P} = \bar{P}/\bar{P}_{\text{critical}}$, and normalized deflection $w_{\max}/h$, are identical to those in the previous problem, Section 4.4.4. Fig. 13 depicts plots of the post-buckling response of the laminated composite plates for different boundary conditions using IGA-TSDT model with von Kármán nonlinearity. The initial buckling strength $\bar{P}_{\text{critical}} = P_{\text{critical}} b^2/E_2 h^3$ of the plates for different boundary conditions SSSS, SSSF, FSSS, SFSF, CCCF, CFCF, CFFC, and CFFF is 37.1875, 14.6629, 29.2266, 5.7219, 34.0197, 21.5856, 9.1742, and 1.3302, respectively. In the case of different boundary conditions, the nonlinear eigenvalue - linear buckling approach accurately captures the post-buckling response of the laminated composite plate up to $w_{\max}/h = 1$. The mode shapes shown in Fig. 13 are from the nonlinear buckling approach.

4.4.6. Effect of fiber orientation on nonlinear buckling response

The influence of fiber orientation on the post-buckling characteristics of angle-ply $(\theta/-\theta)$ laminated plate is now examined. A simply supported (SSSS) thin $(b/h = 100)$ square laminated plate subjected to uniform uniaxial loads is employed. The plate is made of MM2 material properties.

The same normalized load $\hat{P} = \bar{P}/\bar{P}_{\text{critical}}$ and normalized maximum deflection $w_{\max}/h$ are used for the load-deflection plots in Fig. 14 for different laminate stacking sequence $(15°/-15°)$, $(30°/-30°)$, $(45°/-45°)$, $(60°/-60°)$, and $(75°/-75°)$. The present solutions are obtained for IGA-TSDT model using both nonlinear buckling and nonlinear eigenvalue approaches with von Kármán nonlinearity. The initial buckling strength $\bar{P}_{\text{critical}} = P_{\text{critical}} b^2/E_2 h^3$ using linear buckling approach for plates with the following stacking sequence $(15°/-15°)$, $(30°/-30°)$, $(45°/-45°)$, $(60°/-60°)$, and $(75°/-75°)$ is 26.5240, 19.7367, 33.0916, 41.5325, and 26.8976, respectively. It is observed that the angle-ply composite plates do not exhibit pure bifurcation. They initially define bend before following the secondary path as shown in Fig. 16. The post-buckling deflection profiles depend upon the fiber orientation as plates with stacking sequence lamination $(45°/-45°)$, $(60°/-60°)$ and $(75°/-75°)$ buckle with second buckling mode. It is worth mentioning that the actual buckling strengths of the angle-ply laminates are not equal to those predicted by linear buckling approaches. The mode shapes of the angle-ply laminated composite plates for nonlinear eigenvalue and nonlinear buckling approaches are shown in Figs. 15 and 16, respectively.

5. Conclusion

In this paper, two isogeometric plate models that are based on the Reddy's third-order shear deformation theory (TSDT) and unconstrained third-order shear deformation theory (UTSDT) for linear and nonlinear buckling analysis of laminated composite plates are proposed for linear and nonlinear buckling analysis of laminated plates. The plate models make use of NURBS basis functions which inherently satisfy the C^1 continuity of TSDT, making the C^2 IGA-TSDT model a computationally efficient plate model with five DOF. The C^2 IGA-TSDT is found to be superior to C^0 FEM-TSDT in terms of performance and computational cost. Particularly, no tertiary response (path) is observed using C^2 IGA-TSDT. While the accuracy of C^2 IGA-TSDT model is observed to be comparable to that of C^2 IGA-UTSDT, the latter permits higher accuracy at the expense of higher computation cost.

The present isogeometric formulation for nonlinear buckling approach is systematically derived without any presumptions about stress distribution, thus making it applicable to a general buckling problems of composite plate structures. The following conclusions, which are generally in agreement with the FEM study [1], are inferred from the study:

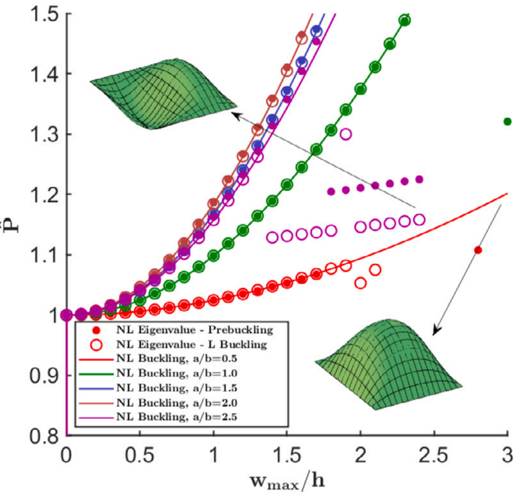

(a) $a/b = 0.5, 1, 1.5, 2, 2.5.$

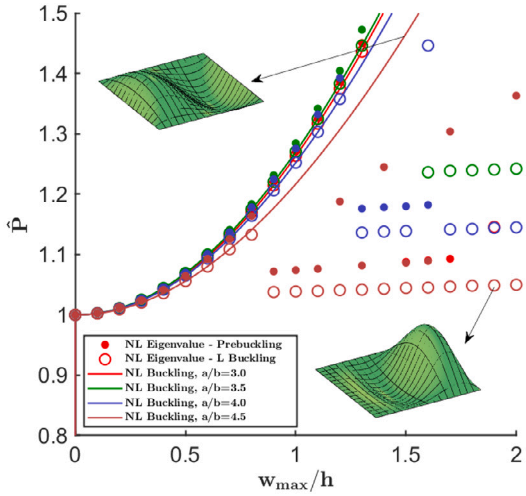

(b) $a/b = 3, 3.5, 4, 4.5.$

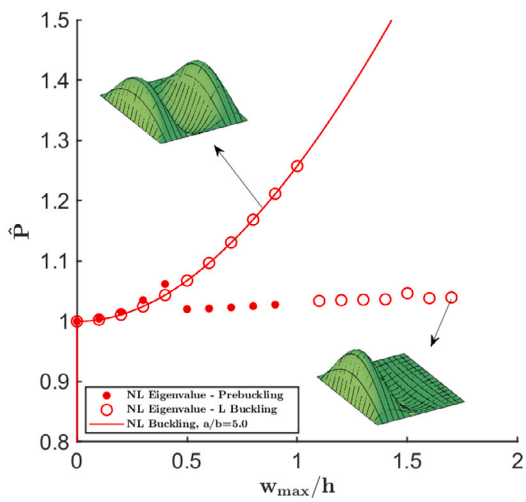

(c) $a/b = 5.$

Fig. 12. Effect of aspect ratio a/b on post-buckling response of simply supported (SSSS) rectangular laminated (0°/90°/0°) plate with $b/h = 100$.

1. The nonlinear eigenvalue approach combined with linear buckling approach is computational cheaper than the nonlinear buckling approach and it can be utilized for an accurately predicting the buckling response of symmetric cross-ply laminated plates for $w_{\max}/h < 0.9$.
2. Nonlinear eigenvalue approach and linear buckling approach are limited to only symmetric cross-ply laminated plates. The angle-ply laminated composite plates do not exhibit pure bifurcation but a bending-buckling response.
3. The boundary conditions used in the pre-buckling analysis significantly influence the accuracy of the linear eigenvalue buckling analysis. For realistic predictions of buckling analysis, as verified via the nonlinear buckling approach, it is suggested to use buckling boundary conditions in pre-buckling analysis, as done in the linear buckling approach.
4. Regarding stress stiffening effect, Green-Lagrange nonlinearity captures the contributions of inplane displacements and predicts more accurate buckling strengths under different types of inplane loads. Thus, it is suggested to incorporate Green-Lagrange stress stiffening in the formulation for better design and reliability of composite plate structures, particularly for moderately thick structures.

The use of higher-order shear deformation may not fully capture thickness stretching effect, which is important for accurate prediction of the critical buckling temperature in thermal buckling analysis. Future studies could employ higher-order shear and normal shear deformation theories to enhance the capability of the present model.

CRediT authorship contribution statement

Surendra Verma: Writing – original draft, Visualization, Validation, Software, Methodology, Investigation, Data curation, Conceptualization. **Abha Gupta:** Visualization, Software, Methodology. **Rabindra Prasad:** Visualization, Software. **Donatus Oguamanam:** Writing – review & editing, Supervision, Resources.

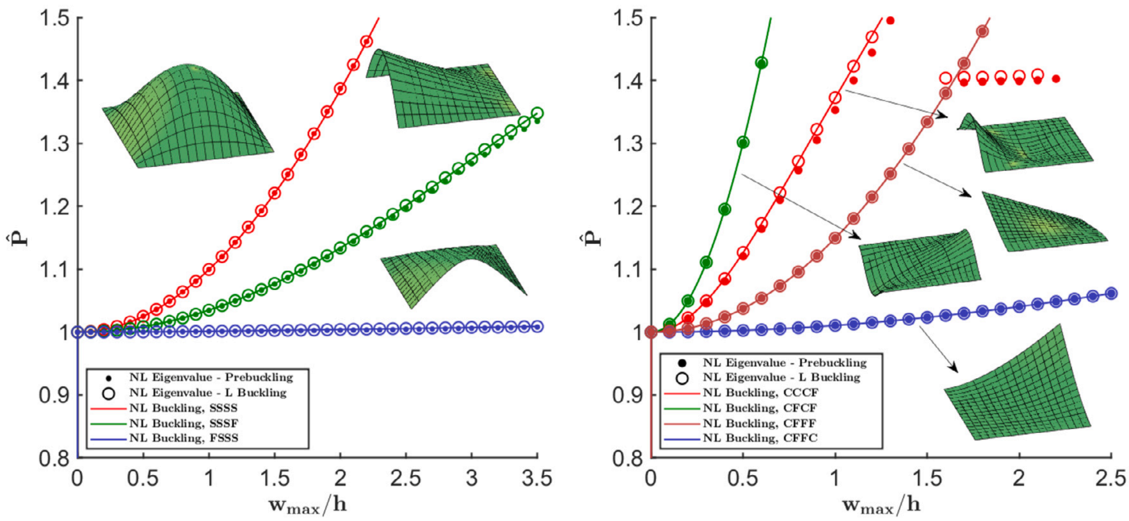

(a) SSSS, SSSF, FSSS, SFSF. **(b)** CCCF, CFCF, CFFC, CFFF.

Fig. 13. Effect of boundary conditions on post-buckling response of square laminated (0°/90°/90°/0°) plate under uniform uniaxial loads.

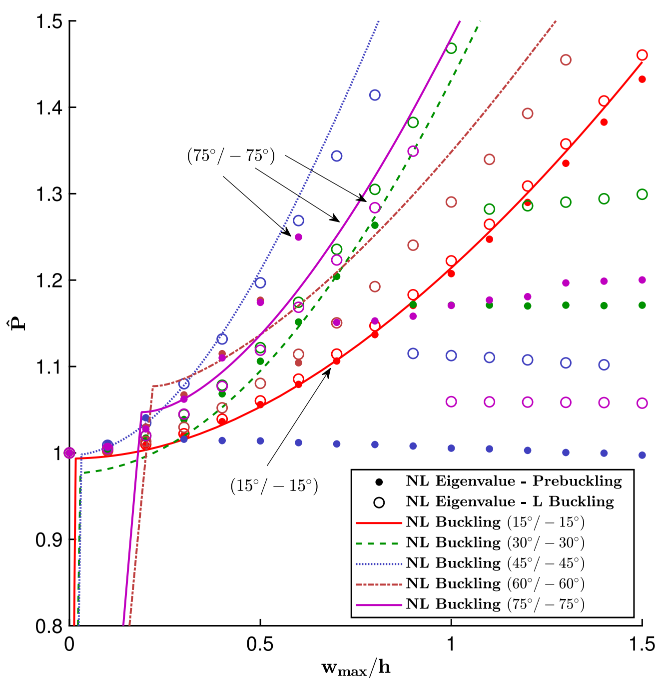

Fig. 14. Effect of fiber orientation on post-buckling response of square $(\theta°/-\theta°)$ plates under uniform uniaxial loads.

Declaration of competing interest

The authors declare that they have no known competing financial interests or personal relationships that could have appeared to influence the work reported in this paper.

Data availability

Data will be made available on request.

Appendix A. Expression of thickness matrices and generalized strains for UTSDT

$$Z_{lb} = \begin{bmatrix} 1 & 0 & 0 & z & 0 & 0 & z^2 & 0 & 0 & z^3 & 0 & 0 \\ 0 & 1 & 0 & 0 & z & 0 & 0 & z^2 & 0 & 0 & z^3 & 0 \\ 0 & 0 & 1 & 0 & 0 & z & 0 & 0 & z^2 & 0 & 0 & z^3 \end{bmatrix} \tag{A.1a}$$

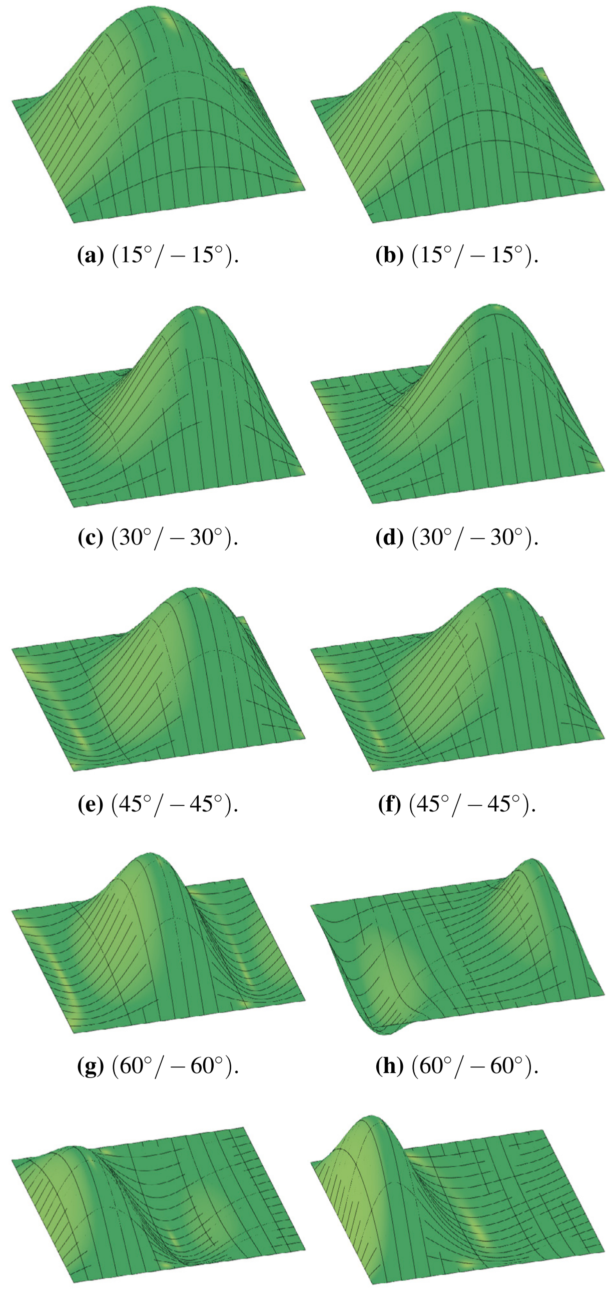

(a) $(15^\circ/-15^\circ)$. **(b)** $(15^\circ/-15^\circ)$.

(c) $(30^\circ/-30^\circ)$. **(d)** $(30^\circ/-30^\circ)$.

(e) $(45^\circ/-45^\circ)$. **(f)** $(45^\circ/-45^\circ)$.

(g) $(60^\circ/-60^\circ)$. **(h)** $(60^\circ/-60^\circ)$.

(i) $(75^\circ/-75^\circ)$. **(j)** $(75^\circ/-75^\circ)$.

Fig. 15. Post-buckling response of square laminated $(\theta^\circ/-\theta^\circ)$ plates using nonlinear eigenvalue - prebuckling approach (left) and Nonlinear eigenvalue - linear buckling approach (right).

$$\boldsymbol{Z}_{ls} = \begin{bmatrix} 1 & 0 & z & 0 & z^2 & 0 \\ 0 & 1 & 0 & z & 0 & z^2 \end{bmatrix} \tag{A.1b}$$

$$\hat{\boldsymbol{\varepsilon}}_{lb} = \left\{ \frac{\partial u_0}{\partial x} \;\; \frac{\partial v_0}{\partial y} \;\; \frac{\partial u_0}{\partial y} + \frac{\partial v_0}{\partial x} \;\; \frac{\partial \phi_x}{\partial x} \;\; \frac{\partial \phi_y}{\partial y} \;\; \frac{\partial \phi_y}{\partial x} + \frac{\partial \phi_x}{\partial y} \;\; \frac{\partial \theta_x}{\partial x} \;\; \frac{\partial \theta_y}{\partial y} \;\; \frac{\partial \theta_x}{\partial y} + \frac{\partial \theta_y}{\partial x} \;\; \frac{\partial \psi_x}{\partial x} \;\; \frac{\partial \psi_y}{\partial y} \;\; \frac{\partial \psi_x}{\partial y} + \frac{\partial \psi_y}{\partial x} \right\}^T \tag{A.1c}$$

$$\hat{\boldsymbol{\varepsilon}}_{ls} = \left\{ \frac{\partial w_0}{\partial y} + \phi_y \;\; \frac{\partial w_0}{\partial x} + \phi_x \;\; 2\theta_y \;\; 2\theta_x \;\; 3\psi_y \;\; 3\psi_x \right\}^T \tag{A.1d}$$

$$\boldsymbol{Z}_{nlb} = \begin{bmatrix} 1 & 0 & 0 & z & 0 & 0 & z^2 & 0 & 0 & z^3 & 0 & 0 & z^4 & 0 & 0 & z^5 & 0 & 0 & z^6 & 0 & 0 \\ 0 & 1 & 0 & 0 & z & 0 & 0 & z^2 & 0 & 0 & z^3 & 0 & 0 & z^4 & 0 & 0 & z^5 & 0 & 0 & z^6 & 0 \\ 0 & 0 & 1 & 0 & 0 & z & 0 & 0 & z^2 & 0 & 0 & z^3 & 0 & 0 & z^4 & 0 & 0 & z^5 & 0 & 0 & z^6 \end{bmatrix} \tag{A.2a}$$

$$\boldsymbol{Z}_{nls} = \begin{bmatrix} 1 & 0 & z & 0 & z^2 & 0 & z^3 & 0 & z^4 & 0 & z^5 & 0 \\ 0 & 1 & 0 & z & 0 & z^2 & 0 & z^3 & 0 & z^4 & 0 & z^5 \end{bmatrix} \tag{A.2b}$$

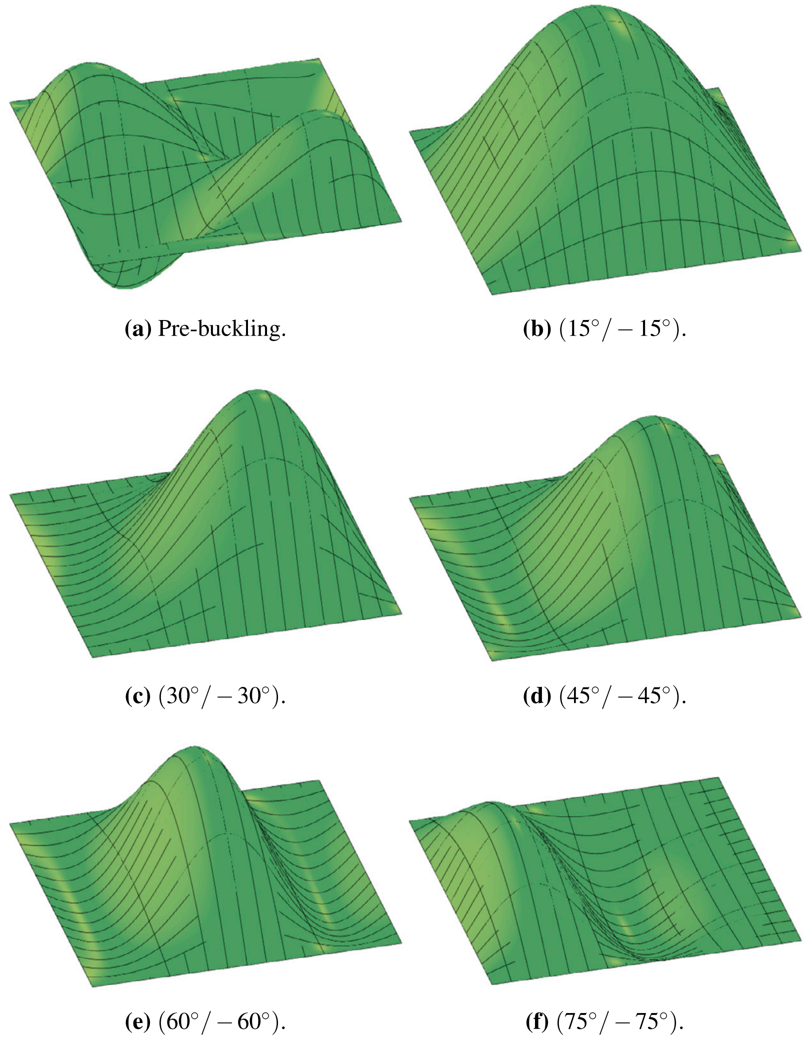

Fig. 16. Pre-buckling and post-buckling response of square laminated $(\theta^\circ/-\theta^\circ)$ plates using nonlinear buckling approach.

$$\boldsymbol{\phi}_b = \left\{ \frac{\partial u_0}{\partial x} \; \frac{\partial u_0}{\partial y} \; \frac{\partial v_0}{\partial x} \; \frac{\partial v_0}{\partial y} \; \frac{\partial w_0}{\partial x} \; \frac{\partial w_0}{\partial y} \; \frac{\partial \phi_x}{\partial x} \; \frac{\partial \phi_x}{\partial y} \; \frac{\partial \phi_y}{\partial x} \; \frac{\partial \phi_y}{\partial y} \; \frac{\partial \theta_x}{\partial x} \; \frac{\partial \theta_x}{\partial y} \; \frac{\partial \theta_y}{\partial x} \; \frac{\partial \theta_y}{\partial y} \; \frac{\partial \psi_x}{\partial x} \; \frac{\partial \psi_x}{\partial y} \; \frac{\partial \psi_y}{\partial x} \; \frac{\partial \psi_y}{\partial y} \right\}^T \tag{A.2c}$$

$$\boldsymbol{\phi}_s = \left\{ \phi_x \; \phi_y \; \theta_x \; \theta_y \; \psi_x \; \psi_y \; \frac{\partial u_0}{\partial x} \; \frac{\partial u_0}{\partial y} \; \frac{\partial v_0}{\partial x} \; \frac{\partial v_0}{\partial y} \; \frac{\partial \phi_x}{\partial x} \; \frac{\partial \phi_x}{\partial y} \; \frac{\partial \phi_y}{\partial x} \; \frac{\partial \phi_y}{\partial y} \; \frac{\partial \theta_x}{\partial x} \; \frac{\partial \theta_x}{\partial y} \; \frac{\partial \theta_y}{\partial x} \; \frac{\partial \theta_y}{\partial y} \; \frac{\partial \psi_x}{\partial x} \; \frac{\partial \psi_x}{\partial y} \; \frac{\partial \psi_y}{\partial x} \; \frac{\partial \psi_y}{\partial y} \right\}^T \tag{A.2d}$$

Appendix B. Expression of generalized stresses for UTSDT

$$\begin{bmatrix} N_{xx} & M_{xx} & P_{xx} & Q_{xx} & R_{xx} & S_{xx} & T_{xx} \\ N_{yy} & M_{yy} & P_{yy} & Q_{yy} & R_{yy} & S_{yy} & T_{yy} \\ N_{xy} & M_{xy} & P_{xy} & Q_{xy} & R_{xy} & S_{xy} & T_{xy} \end{bmatrix} = \int_{-h/2}^{h/2} \begin{Bmatrix} \sigma_{xx} \\ \sigma_{yy} \\ \tau_{xy} \end{Bmatrix} \left\{ 1 \;\; z \;\; z^2 \;\; z^3 \;\; z^4 \;\; z^5 \;\; z^6 \right\} dz$$

$$\begin{bmatrix} N_{yz} & M_{yz} & P_{yz} & Q_{yz} & R_{yz} & S_{yz} \\ N_{xz} & M_{xz} & P_{xz} & Q_{xz} & R_{xz} & S_{xz} \end{bmatrix} = \int_{-h/2}^{h/2} \begin{Bmatrix} \tau_{yz} \\ \tau_{xz} \end{Bmatrix} \left\{ 1 \;\; z \;\; z^2 \;\; z^3 \;\; z^4 \;\; z^5 \right\} dz$$

Appendix C. Expression of $\mathbb{N}_b$ and $\mathbb{N}_s$ for UTSDT

$$
\mathbb{N}_b = \begin{bmatrix}
N_{xx} & N_{xy} & 0 & 0 & 0 & 0 & M_{xx} & M_{xy} & 0 & 0 & P_{xx} & P_{xy} & 0 & 0 & Q_{xx} & Q_{xy} & 0 & 0 \\
N_{xy} & N_{yy} & 0 & 0 & 0 & 0 & M_{xy} & M_{yy} & 0 & 0 & P_{xy} & P_{yy} & 0 & 0 & Q_{xy} & Q_{yy} & 0 & 0 \\
0 & 0 & N_{xx} & N_{xy} & 0 & 0 & 0 & 0 & M_{xx} & M_{xy} & 0 & 0 & P_{xx} & P_{xy} & 0 & 0 & Q_{xx} & Q_{xy} \\
0 & 0 & N_{xy} & N_{yy} & 0 & 0 & 0 & 0 & M_{xy} & M_{yy} & 0 & 0 & P_{xy} & P_{yy} & 0 & 0 & Q_{xy} & Q_{yy} \\
0 & 0 & 0 & 0 & N_{xx} & N_{xy} & 0 & 0 & 0 & 0 & 0 & 0 & 0 & 0 & 0 & 0 & 0 & 0 \\
0 & 0 & 0 & 0 & N_{xy} & N_{yy} & 0 & 0 & 0 & 0 & 0 & 0 & 0 & 0 & 0 & 0 & 0 & 0 \\
M_{xx} & M_{xy} & 0 & 0 & 0 & 0 & P_{xx} & P_{xy} & 0 & 0 & Q_{xx} & Q_{xy} & 0 & 0 & R_{xx} & R_{xy} & 0 & 0 \\
M_{xy} & M_{yy} & 0 & 0 & 0 & 0 & P_{xy} & P_{yy} & 0 & 0 & Q_{xy} & Q_{yy} & 0 & 0 & R_{xy} & R_{yy} & 0 & 0 \\
0 & 0 & M_{xx} & M_{xy} & 0 & 0 & 0 & 0 & P_{xx} & P_{xy} & 0 & 0 & Q_{xx} & Q_{xy} & 0 & 0 & R_{xx} & R_{xy} \\
0 & 0 & M_{xy} & M_{yy} & 0 & 0 & 0 & 0 & P_{xy} & P_{yy} & 0 & 0 & Q_{xy} & Q_{yy} & 0 & 0 & R_{xy} & R_{yy} \\
P_{xx} & P_{xy} & 0 & 0 & 0 & 0 & Q_{xx} & Q_{xy} & 0 & 0 & R_{xx} & R_{xy} & 0 & 0 & S_{xx} & S_{xy} & 0 & 0 \\
P_{xy} & P_{yy} & 0 & 0 & 0 & 0 & Q_{xy} & Q_{yy} & 0 & 0 & R_{xy} & R_{yy} & 0 & 0 & S_{xy} & S_{yy} & 0 & 0 \\
0 & 0 & P_{xx} & P_{xy} & 0 & 0 & 0 & 0 & Q_{xx} & Q_{xy} & 0 & 0 & R_{xx} & R_{xy} & 0 & 0 & S_{xx} & S_{xy} \\
0 & 0 & P_{xy} & P_{yy} & 0 & 0 & 0 & 0 & Q_{xy} & Q_{yy} & 0 & 0 & R_{xy} & R_{yy} & 0 & 0 & S_{xy} & S_{yy} \\
Q_{xx} & Q_{xy} & 0 & 0 & 0 & 0 & R_{xx} & R_{xy} & 0 & 0 & S_{xx} & S_{xy} & 0 & 0 & T_{xx} & T_{xy} & 0 & 0 \\
Q_{xy} & Q_{yy} & 0 & 0 & 0 & 0 & R_{xy} & R_{yy} & 0 & 0 & S_{xy} & S_{yy} & 0 & 0 & T_{xy} & T_{yy} & 0 & 0 \\
0 & 0 & Q_{xx} & Q_{xy} & 0 & 0 & 0 & 0 & R_{xx} & R_{xy} & 0 & 0 & S_{xx} & S_{xy} & 0 & 0 & T_{xx} & T_{xy} \\
0 & 0 & Q_{xy} & Q_{yy} & 0 & 0 & 0 & 0 & R_{xy} & R_{yy} & 0 & 0 & S_{xy} & S_{yy} & 0 & 0 & T_{xy} & T_{yy}
\end{bmatrix}
$$

$$
\mathbb{N}_s = \begin{bmatrix}
0 & 0 & 0 & 0 & 0 & 0 & N_{xz} & N_{yz} & 0 & 0 & M_{xz} & M_{yz} & 0 & 0 & P_{xz} & P_{yz} & 0 & 0 & Q_{xz} & Q_{yz} & 0 & 0 \\
0 & 0 & 0 & 0 & 0 & 0 & 0 & 0 & N_{xz} & N_{yz} & 0 & 0 & M_{xz} & M_{yz} & 0 & 0 & P_{xz} & P_{yz} & 0 & 0 & Q_{xz} & Q_{yz} \\
0 & 0 & 0 & 0 & 0 & 0 & 2M_{xz} & 2M_{yz} & 0 & 0 & 2P_{xz} & 2P_{yz} & 0 & 0 & 2Q_{xz} & 2Q_{yz} & 0 & 0 & 2R_{xz} & 2R_{yz} & 0 & 0 \\
0 & 0 & 0 & 0 & 0 & 0 & 0 & 0 & 2M_{xz} & 2M_{yz} & 0 & 0 & 2P_{xz} & 2P_{yz} & 0 & 0 & 2Q_{xz} & 2Q_{yz} & 0 & 0 & 2R_{xz} & 2R_{yz} \\
0 & 0 & 0 & 0 & 0 & 0 & 3P_{xz} & 3P_{yz} & 0 & 0 & 3Q_{xz} & 3Q_{yz} & 0 & 0 & 3R_{xz} & 3R_{yz} & 0 & 0 & 3S_{xz} & 3S_{yz} & 0 & 0 \\
0 & 0 & 0 & 0 & 0 & 0 & 0 & 0 & 3P_{xz} & 3P_{yz} & 0 & 0 & 3Q_{xz} & 3Q_{yz} & 0 & 0 & 3R_{xz} & 3R_{yz} & 0 & 0 & 3S_{xz} & 3S_{yz} \\
N_{xz} & 0 & 2M_{xz} & 0 & 3P_{xz} & 0 & 0 & 0 & 0 & 0 & 0 & 0 & 0 & 0 & 0 & 0 & 0 & 0 & 0 & 0 & 0 & 0 \\
N_{yz} & 0 & 2M_{yz} & 0 & 3P_{yz} & 0 & 0 & 0 & 0 & 0 & 0 & 0 & 0 & 0 & 0 & 0 & 0 & 0 & 0 & 0 & 0 & 0 \\
0 & N_{xz} & 0 & 2M_{xz} & 0 & 3P_{xz} & 0 & 0 & 0 & 0 & 0 & 0 & 0 & 0 & 0 & 0 & 0 & 0 & 0 & 0 & 0 & 0 \\
0 & N_{yz} & 0 & 2M_{yz} & 0 & 3P_{yz} & 0 & 0 & 0 & 0 & 0 & 0 & 0 & 0 & 0 & 0 & 0 & 0 & 0 & 0 & 0 & 0 \\
M_{xz} & 0 & 2P_{xz} & 0 & 3Q_{xz} & 0 & 0 & 0 & 0 & 0 & 0 & 0 & 0 & 0 & 0 & 0 & 0 & 0 & 0 & 0 & 0 & 0 \\
M_{yz} & 0 & 2P_{yz} & 0 & 3Q_{yz} & 0 & 0 & 0 & 0 & 0 & 0 & 0 & 0 & 0 & 0 & 0 & 0 & 0 & 0 & 0 & 0 & 0 \\
0 & M_{xz} & 0 & 2P_{xz} & 0 & 3Q_{xz} & 0 & 0 & 0 & 0 & 0 & 0 & 0 & 0 & 0 & 0 & 0 & 0 & 0 & 0 & 0 & 0 \\
0 & M_{yz} & 0 & 2P_{yz} & 0 & 3Q_{yz} & 0 & 0 & 0 & 0 & 0 & 0 & 0 & 0 & 0 & 0 & 0 & 0 & 0 & 0 & 0 & 0 \\
P_{xz} & 0 & 2Q_{xz} & 0 & 3R_{xz} & 0 & 0 & 0 & 0 & 0 & 0 & 0 & 0 & 0 & 0 & 0 & 0 & 0 & 0 & 0 & 0 & 0 \\
P_{yz} & 0 & 2Q_{yz} & 0 & 3R_{yz} & 0 & 0 & 0 & 0 & 0 & 0 & 0 & 0 & 0 & 0 & 0 & 0 & 0 & 0 & 0 & 0 & 0 \\
0 & P_{xz} & 0 & 2Q_{xz} & 0 & 3R_{xz} & 0 & 0 & 0 & 0 & 0 & 0 & 0 & 0 & 0 & 0 & 0 & 0 & 0 & 0 & 0 & 0 \\
0 & P_{yz} & 0 & 2Q_{yz} & 0 & 3R_{yz} & 0 & 0 & 0 & 0 & 0 & 0 & 0 & 0 & 0 & 0 & 0 & 0 & 0 & 0 & 0 & 0 \\
Q_{xz} & 0 & 2R_{xz} & 0 & 3S_{xz} & 0 & 0 & 0 & 0 & 0 & 0 & 0 & 0 & 0 & 0 & 0 & 0 & 0 & 0 & 0 & 0 & 0 \\
Q_{yz} & 0 & 2R_{yz} & 0 & 3S_{yz} & 0 & 0 & 0 & 0 & 0 & 0 & 0 & 0 & 0 & 0 & 0 & 0 & 0 & 0 & 0 & 0 & 0 \\
0 & Q_{xz} & 0 & 2R_{xz} & 0 & 3S_{xz} & 0 & 0 & 0 & 0 & 0 & 0 & 0 & 0 & 0 & 0 & 0 & 0 & 0 & 0 & 0 & 0 \\
0 & Q_{yz} & 0 & 2R_{yz} & 0 & 3S_{yz} & 0 & 0 & 0 & 0 & 0 & 0 & 0 & 0 & 0 & 0 & 0 & 0 & 0 & 0 & 0 & 0
\end{bmatrix}
$$

Appendix D. Navier solution for simply supported anti-symmetric cross-ply composite plate under inplane mechanical loads for UTSDT

$$u_0 = \sum_{m=1}^{\infty}\sum_{n=1}^{\infty} u_{0mn} cos\,(\alpha x)\, sin\,(\beta y) \qquad v_0 = \sum_{m=1}^{\infty}\sum_{n=1}^{\infty} v_{0mn} sin\,(\alpha x)\, cos\,(\beta y)$$

$$w_0 = \sum_{m=1}^{\infty}\sum_{n=1}^{\infty} w_{0mn} sin\,(\alpha x)\, sin\,(\beta y)$$

$$\phi_x = \sum_{m=1}^{\infty}\sum_{n=1}^{\infty} \phi_{xmn} cos\,(\alpha x)\, sin\,(\beta y) \qquad \phi_y = \sum_{m=1}^{\infty}\sum_{n=1}^{\infty} \phi_{ymn} sin\,(\alpha x)\, cos\,(\beta y)$$

$$\theta_x = \sum_{m=1}^{\infty}\sum_{n=1}^{\infty} \theta_{xmn} sin\,(\alpha x)\, cos\,(\beta y) \qquad \theta_y = \sum_{m=1}^{\infty}\sum_{n=1}^{\infty} \theta_{ymn} cos\,(\alpha x)\, sin\,(\beta y)$$

$$\psi_x = \sum_{m=1}^{\infty}\sum_{n=1}^{\infty} \psi_{xmn} sin\,(\alpha x)\, cos\,(\beta y) \qquad \psi_y = \sum_{m=1}^{\infty}\sum_{n=1}^{\infty} \psi_{ymn} cos\,(\alpha x)\, sin\,(\beta y)$$

$$\left(\begin{bmatrix} K_{11} & K_{12} & K_{13} & K_{14} & K_{15} & K_{16} & K_{17} & K_{18} & K_{19} \\ & K_{22} & K_{23} & K_{24} & K_{25} & K_{26} & K_{27} & K_{28} & K_{29} \\ & & K_{33} & K_{34} & K_{35} & K_{36} & K_{37} & K_{38} & K_{39} \\ & & & K_{44} & K_{45} & K_{46} & K_{47} & K_{48} & K_{49} \\ & & & & K_{55} & K_{56} & K_{57} & K_{58} & K_{59} \\ & & & & & K_{66} & K_{67} & K_{68} & K_{69} \\ & & \text{sym} & & & & K_{77} & K_{78} & K_{79} \\ & & & & & & & K_{88} & K_{89} \\ & & & & & & & & K_{99} \end{bmatrix} - \lambda \begin{bmatrix} 0 & 0 & 0 & 0 & 0 & 0 & 0 & 0 & 0 \\ & 0 & 0 & 0 & 0 & 0 & 0 & 0 & 0 \\ & & K_{33}^{g} & 0 & 0 & 0 & 0 & 0 & 0 \\ & & & 0 & 0 & 0 & 0 & 0 & 0 \\ & & & & 0 & 0 & 0 & 0 & 0 \\ & & & & & 0 & 0 & 0 & 0 \\ & & \text{sym} & & & & 0 & 0 & 0 \\ & & & & & & & 0 & 0 \\ & & & & & & & & 0 \end{bmatrix}\right) \begin{Bmatrix} u_{0mn} \\ v_{0mn} \\ w_{0mn} \\ \phi_{xmn} \\ \phi_{ymn} \\ \theta_{xmn} \\ \theta_{ymn} \\ \psi_{xmn} \\ \psi_{ymn} \end{Bmatrix} = \begin{Bmatrix} 0 \\ 0 \\ 0 \\ 0 \\ 0 \\ 0 \\ 0 \\ 0 \\ 0 \end{Bmatrix}$$

$$\begin{aligned}
K_{11} &= \alpha^2 A_{11} + \beta^2 A_{66} & K_{12} &= \alpha\beta\left(A_{12} + A_{66}\right) \\
K_{14} &= \alpha^2 B_{11} + \beta^2 B_{66} & K_{15} &= \alpha\beta\left(B_{12} + B_{66}\right) \\
K_{16} &= \alpha^2 C_{11} + \beta^2 C_{66} & K_{17} &= \alpha\beta\left(C_{12} + C_{66}\right) \\
K_{18} &= \alpha D_{11} + \beta^2 D_{66} & K_{19} &= \alpha\beta\left(D_{12} + D_{66}\right) \\
K_{22} &= \alpha^2 A_{66} + \beta^2 A_{22} & K_{24} &= \alpha\beta\left(B_{12} + B_{66}\right) \\
K_{25} &= \alpha^2 B_{66} + \beta^2 B_{22} & K_{26} &= \alpha\beta\left(C_{12} + C_{66}\right) \\
K_{27} &= \alpha^2 C_{66} + \beta^2 C_{22} & K_{28} &= \alpha\beta\left(D_{12} + D_{66}\right) \\
K_{29} &= \alpha^2 D_{66} + \beta^2 D_{22} & K_{33} &= \alpha^2 A_{55} + \beta^2 A_{44} \\
K_{34} &= \alpha A_{55} & K_{35} &= \beta A_{44} \\
K_{36} &= \alpha B_{55} & K_{37} &= \beta B_{44} \\
K_{38} &= \alpha C_{55} & K_{39} &= \beta C_{44} \\
K_{44} &= \alpha^2 E_{11} + \beta^2 E_{66} + A_{55} & K_{45} &= \alpha\beta\left(E_{12} + E_{66}\right) \\
K_{46} &= \alpha^2 F_{11} + \beta^2 F_{66} + B_{55} & K_{47} &= \alpha\beta\left(F_{12} + F_{66}\right) \\
K_{48} &= \alpha^2 G_{11} + \beta^2 G_{66} + C_{55} & K_{49} &= \alpha\beta\left(G_{12} + G_{66}\right) \\
K_{55} &= \alpha^2 E_{66} + \beta^2 E_{22} + A_{44} & K_{56} &= \alpha\beta\left(F_{12} + F_{66}\right) \\
K_{57} &= \alpha^2 F_{66} + \beta^2 F_{22} + B_{44} & K_{58} &= \alpha\beta\left(G_{12} + G_{66}\right) \\
K_{59} &= \alpha^2 G_{66} + \beta^2 G_{22} + C_{44} & & \\
K_{66} &= \alpha^2 H_{11} + \beta^2 H_{66} + D_{55} & K_{67} &= \alpha\beta\left(H_{12} + H_{66}\right) \\
K_{68} &= \alpha^2 I_{11} + \beta^2 I_{66} + E_{55} & K_{69} &= \alpha\beta\left(I_{12} + I_{66}\right) \\
K_{77} &= \alpha^2 H_{66} + \beta^2 H_{22} + D_{44} & K_{78} &= \alpha\beta\left(I_{12} + I_{66}\right) \\
K_{79} &= \alpha^2 I_{66} + \beta^2 I_{22} + E_{44} & & \\
K_{88} &= \alpha^2 J_{11} + \beta^2 J_{66} + F_{55} & K_{89} &= \alpha\beta\left(J_{12} + J_{66}\right) \\
K_{99} &= \alpha^2 J_{66} + \beta^2 J_{22} + F_{44} & K_{33}^{g} &= K_{33}^{gm}
\end{aligned}$$

$$\begin{aligned}
K_{33}^{gm} &= \alpha^2 && \text{Uniaxial uniform loading in x-direction} \\
K_{33}^{gm} &= \beta^2 && \text{Uniaxial uniform loading in y-direction} \\
K_{33}^{gm} &= \alpha^2 + \left(N_y/N_x\right)\beta^2 && \text{Biaxial uniform loading in both directions}
\end{aligned}$$

$$\left[A_{ij}\right] = \int_{-h/2}^{h/2} \bar{Q}_{ij}\,dz \qquad \left[B_{ij}\right] = \int_{-h/2}^{h/2} 2z\bar{Q}_{ij}\,dz \qquad \left[C_{ij}\right] = \int_{-h/2}^{h/2} 3z^2\bar{Q}_{ij}\,dz$$

$$\left[D_{ij}\right] = \int_{-h/2}^{h/2} 4z^2\bar{Q}_{ij}\,dz \qquad \left[E_{ij}\right] = \int_{-h/2}^{h/2} 6z^3\bar{Q}_{ij}\,dz \qquad \left[F_{ij}\right] = \int_{-h/2}^{h/2} 9z^4\bar{Q}_{ij}\,dz$$

$$i, j = 4, 5$$

$$\left[A_{ij}\right] = \int_{-h/2}^{h/2} \bar{Q}_{ij}\,dz \qquad \left[B_{ij}\right] = \int_{-h/2}^{h/2} z\bar{Q}_{ij}\,dz \qquad \left[C_{ij}\right] = \int_{-h/2}^{h/2} z^2\bar{Q}_{ij}\,dz$$

$$\left[D_{ij}\right] = \int_{-h/2}^{h/2} z^3\bar{Q}_{ij}\,dz \qquad \left[E_{ij}\right] = \int_{-h/2}^{h/2} z^2\bar{Q}_{ij}\,dz \qquad \left[F_{ij}\right] = \int_{-h/2}^{h/2} z^3\bar{Q}_{ij}\,dz$$

$$[G_{ij}] = \int_{-h/2}^{h/2} z^4 \bar{Q}_{ij} dz \qquad [H_{ij}] = \int_{-h/2}^{h/2} z^4 \bar{Q}_{ij} dz \qquad [I_{ij}] = \int_{-h/2}^{h/2} z^5 \bar{Q}_{ij} dz$$

$$[J_{ij}] = \int_{-h/2}^{h/2} z^6 \bar{Q}_{ij} dz \qquad i,j = 1,2,6$$

Lowest buckling load (λ) is obtained by considering Navier solution for $m = n = 1$.

References

[1] S. Verma, A. Gupta, B.R. Thakur, D. Oguamanam, B. Singh, A unified buckling formulation for linear and nonlinear analysis of laminated plates using penalty based c0 fem-hsdt model, Int. J. Non-Linear Mech. (2023) 104619, https://doi.org/10.1016/j.ijnonlinmec.2023.104619.

[2] J.A. Cottrell, T.J.R. Hughes, Y. Bazilevs, Isogeometric Analysis, Wiley, 2009.

[3] S.T. Dennis, A.N. Palazotto, The effect of non-linear curvature strains on the buckling of laminated plates and shells, Int. J. Numer. Methods Eng. 36 (4) (1993) 595–609, https://doi.org/10.1002/nme.1620360404.

[4] A.K. Ghosh, S.S. Dey, Buckling of laminated plates - a simple finite element based on higher-order theory, Finite Elem. Anal. Des. 15 (4) (1994) 289–302, https://doi.org/10.1016/0168-874x(94)90023-x.

[5] G. Singh, G. Rao, N. Iyengar, Geometrically nonlinear flexural response characteristics of shear deformable unsymmetrically laminated plates, Comput. Struct. 53 (1) (1994) 69–81, https://doi.org/10.1016/0045-7949(94)90131-7.

[6] P. Sundaresan, G. Singh, G. Rao, Buckling and post-buckling analysis of moderately thick laminated rectangular plates, Comput. Struct. 61 (1) (1996) 79–86, https://doi.org/10.1016/0045-7949(96)00010-7.

[7] I. Shufrin, M. Eisenberger, Stability of variable thickness shear deformable plates—first order and high order analyses, Thin-Walled Struct. 43 (2) (2005) 189–207, https://doi.org/10.1016/j.tws.2004.07.013.

[8] E. Ruocco, V. Minutolo, Buckling analysis of Mindlin plates under the Green–Lagrange strain hypothesis, Int. J. Struct. Stab. Dyn. 15 (06) (2015) 1450079, https://doi.org/10.1142/s0219455414500795.

[9] E. Ruocco, J. Reddy, A closed-form solution for buckling analysis of orthotropic reddy plates and prismatic plate structures, Composites, Part B, Eng. 169 (2019) 258–273, https://doi.org/10.1016/j.compositesb.2019.03.015.

[10] N. Sharma, M. Nishad, D.K. Maiti, M.R. Sunny, B.N. Singh, Uncertainty quantification in buckling strength of variable stiffness laminated composite plate under thermal loading, Compos. Struct. 275 (2021) 114486, https://doi.org/10.1016/j.compstruct.2021.114486.

[11] M. Cetkovic, Influence of initial geometrical imperfections on thermal stability of laminated composite plates using layerwise finite element, Compos. Struct. 291 (2022) 115547, https://doi.org/10.1016/j.compstruct.2022.115547.

[12] C.H. Thai, H. Nguyen-Xuan, N. Nguyen-Thanh, T.H. Le, T. Rabczuk, Static, free vibration, and buckling analysis of laminated composite Reissner-Mindlin plates using NURBS-based isogeometric approach, Int. J. Numer. Methods Eng. 91 (6) (2012) 571–603, https://doi.org/10.1002/nme.4282.

[13] K. Fan, J. Zeng, Z. Huang, Q. Liu, Tensor-decomposition based matrix computation: a fast method for the isogeometric FSDT analysis of laminated composite plate, Thin-Walled Struct. 144 (2019) 106326, https://doi.org/10.1016/j.tws.2019.106326.

[14] C.H. Thai, H. Nguyen-Xuan, S.P.A. Bordas, N. Nguyen-Thanh, T. Rabczuk, Isogeometric analysis of laminated composite plates using the higher-order shear deformation theory, Mech. Adv. Mat. Struct. 22 (6) (2015) 451–469, https://doi.org/10.1080/15376494.2013.779050.

[15] O. Peković, S. Stupar, A. Simonović, J. Svorcan, S. Trivković, Free vibration and buckling analysis of higher order laminated composite plates using the isogeometric approach, J. Theor. Appl. Mech. 453 (2015), https://doi.org/10.15632/jtam-pl.53.2.453.

[16] C.H. Thai, A. Ferreira, S. Bordas, T. Rabczuk, H. Nguyen-Xuan, Isogeometric analysis of laminated composite and sandwich plates using a new inverse trigonometric shear deformation theory, Eur. J. Mech. A, Solids 43 (2014) 89–108, https://doi.org/10.1016/j.euromechsol.2013.09.001.

[17] P. Shi, C. Dong, F. Sun, W. Liu, Q. Hu, A new higher order shear deformation theory for static, vibration and buckling responses of laminated plates with the isogeometric analysis, Compos. Struct. 204 (2018) 342–358, https://doi.org/10.1016/j.compstruct.2018.07.080.

[18] A. Alesadi, M. Galehdari, S. Shojaee, Free vibration and buckling analysis of composite laminated plates using layerwise models based on isogeometric approach and carrera unified formulation, Mech. Adv. Mat. Struct. 25 (12) (2017) 1018–1032, https://doi.org/10.1080/15376494.2017.1342883.

[19] T. Le-Manh, J. Lee, Postbuckling of laminated composite plates using NURBS-based isogeometric analysis, Compos. Struct. 109 (2014) 286–293, https://doi.org/10.1016/j.compstruct.2013.11.011.

[20] S. Shojaee, N. Valizadeh, E. Izadpanah, T. Bui, T.V. Vu, Free vibration and buckling analysis of laminated composite plates using the NURBS-based isogeometric finite element method, Compos. Struct. 94 (5) (2012) 1677–1693, https://doi.org/10.1016/j.compstruct.2012.01.012.

[21] S. Yin, T. Yu, T.Q. Bui, S. Xia, S. Hirose, A cutout isogeometric analysis for thin laminated composite plates using level sets, Compos. Struct. 127 (2015) 152–164, https://doi.org/10.1016/j.compstruct.2015.03.016.

[22] T. Yu, S. Yin, T.Q. Bui, S. Xia, S. Tanaka, S. Hirose, NURBS-based isogeometric analysis of buckling and free vibration problems for laminated composites plates with complicated cutouts using a new simple FSDT theory and level set method, Thin-Walled Struct. 101 (2016) 141–156, https://doi.org/10.1016/j.tws.2015.12.008.

[23] A. Alesadi, M. Galehdari, S. Shojaee, Free vibration and buckling analysis of cross-ply laminated composite plates using carrera's unified formulation based on isogeometric approach, Comput. Struct. 183 (2017) 38–47, https://doi.org/10.1016/j.compstruc.2017.01.013.

[24] H.X. Nguyen, T.D. Hien, J. Lee, H. Nguyen-Xuan, Stochastic buckling behaviour of laminated composite structures with uncertain material properties, Aerosp. Sci. Technol. 66 (2017) 274–283, https://doi.org/10.1016/j.ast.2017.01.028.

[25] H. Atri, S. Shojaee, Analysis of laminated composite plates based on thb-rkpm method using the higher order shear deformation plate theory, Sci. Iran. 26 (4: Special Issue Dedicated to Professor Abolhassan Vafai) (2019) 2057–2078, https://doi.org/10.24200/sci.2019.21417.

[26] J. Huang, N. Nguyen-Thanh, J. Gao, Z. Fan, K. Zhou, Static, free vibration, and buckling analyses of laminated composite plates via an isogeometric meshfree collocation approach, Compos. Struct. 285 (2022) 115011, https://doi.org/10.1016/j.compstruct.2021.115011.

[27] A. Chakrabarti, A.H. Sheikh, Buckling of laminated sandwich plates subjected to partial edge compression, Int. J. Mech. Sci. 47 (3) (2005) 418–436, https://doi.org/10.1016/j.ijmecsci.2005.01.005.

[28] A. Chakrabarti, A.H. Sheikh, Buckling of composite laminates subjected to in-plane partial edge compression using a refined plate theory, J. Reinf. Plast. Compos. 25 (11) (2006) 1189–1204, https://doi.org/10.1177/0731684406066368.

[29] T. Rajanna, S. Banerjee, Y.M. Desai, D. Prabhakara, Effect of boundary conditions and non-uniform edge loads on buckling characteristics of laminated composite panels with and without cutout, Int. J. Comput. Methods Eng. Sci. Mech. 18 (1) (2017) 64–76, https://doi.org/10.1080/15502287.2016.1276350.

[30] T. Rajanna, S. Banerjee, Y.M. Desai, D.L. Prabhakara, Effect of reinforced cutouts and ply-orientations on buckling behavior of composite panels subjected to non-uniform edge loads, Int. J. Struct. Stab. Dyn. 18 (04) (2018) 1850058, https://doi.org/10.1142/s021945541850058x.

[31] B. Adhikari, B.N. Singh, Buckling characteristics of laminated functionally-graded CNT-reinforced composite plate under nonuniform uniaxial and biaxial in-plane edge loads, Int. J. Struct. Stab. Dyn. 20 (02) (2019) 2050022, https://doi.org/10.1142/s0219455420500224.

[32] S.J. Nima, R. Ganesan, Buckling analysis of symmetrically laminated composite plates including the effect of variable pre-stress field using the Ritz method, Eur. J. Mech. A, Solids 90 (2021) 104323, https://doi.org/10.1016/j.euromechsol.2021.104323.

[33] E. Shafei, A. Shirzad, T. Rabczuk, Dynamic stability optimization of laminated composite plates: an isogeometric HSDT formulation and PSO algorithm, Compos. Struct. 280 (2022) 114935, https://doi.org/10.1016/j.compstruct.2021.114935.

[34] S.N. Patel, A.H. Sheikh, Buckling response of laminated composite stiffened plates subjected to partial in-plane edge loading, Int. J. Comput. Methods Eng. Sci. Mech. 17 (5–6) (2016) 322–338, https://doi.org/10.1080/15502287.2016.1231235.

[35] K. Prajapat, S. Ray-Chaudhuri, A. Kumar, Effect of in-plane boundary conditions on elastic buckling behavior of solid and perforated plates, Thin-Walled Struct. 90 (2015) 171–181, https://doi.org/10.1016/j.tws.2014.12.015.
[36] A. Alhajahmad, C. Mittelstedt, Buckling and postbuckling performance of composite fuselage panels with cutouts using continuous streamline fibres, Int. J. Mech. Sci. 212 (2021) 106841, https://doi.org/10.1016/j.ijmecsci.2021.106841.
[37] T. Dey, L. Ramachandra, Computation of worst geometric imperfection profiles of composite cylindrical shell panels by minimizing the non-linear buckling load, Appl. Math. Model. 74 (2019) 483–495, https://doi.org/10.1016/j.apm.2019.04.065.
[38] N.D. Duc, T.Q. Quan, Nonlinear postbuckling of imperfect eccentrically stiffened p-fgm double curved thin shallow shells on elastic foundations in thermal environments, Compos. Struct. 106 (2013) 590–600, https://doi.org/10.1016/j.compstruct.2013.07.010.
[39] N.D. Duc, H.V. Tung, Mechanical and thermal postbuckling of shear-deformable fgm plates with temperature-dependent properties, Mech. Compos. Mater. 46 (5) (2010) 461–476, https://doi.org/10.1007/s11029-010-9163-9.
[40] N.D. Duc, H.V. Tung, Nonlinear analysis of stability for functionally graded cylindrical panels under axial compression, Comput. Mater. Sci. 49 (4) (2010) S313–S316, https://doi.org/10.1016/j.commatsci.2009.12.030.
[41] N.D. Duc, T.Q. Quan, Nonlinear stability analysis of double-curved shallow fgm panels on elastic foundations in thermal environments, Mech. Compos. Mater. 48 (4) (2012) 435–448, https://doi.org/10.1007/s11029-012-9289-z.
[42] N.D. Duc, Nonlinear Static and Dynamic Stability of Functionally Graded Plates and Shells, Vietnam National University Press, Hanoi, 2014.
[43] N.D. Duc, P.T. Thang, Nonlinear buckling of imperfect eccentrically stiffened metal–ceramic–metal s-fgm thin circular cylindrical shells with temperature-dependent properties in thermal environments, Int. J. Mech. Sci. 81 (2014) 17–25, https://doi.org/10.1016/j.ijmecsci.2014.01.016.
[44] T.Q. Quan, N. Dinh Duc, Nonlinear thermal stability of eccentrically stiffened fgm double curved shallow shells, J. Therm. Stresses 40 (2) (2016) 211–236, https://doi.org/10.1080/01495739.2016.1225532.
[45] A. Bhimaraddi, Buckling and post-buckling behavior of laminated plates using the generalized nonlinear formulation, Int. J. Mech. Sci. 34 (9) (1992) 703–715, https://doi.org/10.1016/0020-7403(92)90003-y.
[46] G. Singh, G. Rao, N. Iyengar, Bifurcation buckling of unsymmetrically laminated plates, Compos. Eng. 4 (2) (1994) 181–194, https://doi.org/10.1016/0961-9526(94)90026-4.
[47] K. Liew, J. Wang, M. Tan, S. Rajendran, Postbuckling analysis of laminated composite plates using the mesh-free kp-Ritz method, Comput. Methods Appl. Mech. Eng. 195 (7–8) (2006) 551–570, https://doi.org/10.1016/j.cma.2005.02.004.
[48] S.K. Panda, L.S. Ramachandra, Buckling and postbuckling behavior of cross-ply composite plate subjected to nonuniform in-plane loads, J. Eng. Mech. 137 (9) (2011) 589–597, https://doi.org/10.1061/(asce)em.1943-7889.0000258.
[49] P. Dash, B. Singh, Buckling and post-buckling of laminated composite plates, Mech. Res. Commun. 46 (2012) 1–7, https://doi.org/10.1016/j.mechrescom.2012.08.002.
[50] L.V. Tran, S.E. Kim, Stability analysis of multi-layered plates subjected to partial edge compression with and without initial imperfection, Compos. Struct. 205 (2018) 26–41, https://doi.org/10.1016/j.compstruct.2018.08.065.
[51] M. Ganapathi, M. Touratier, A study on thermal postbuckling behaviour of laminated composite plates using a shear-flexible finite element, Finite Elem. Anal. Des. 28 (2) (1997) 115–135, https://doi.org/10.1016/s0168-874x(97)81955-5.
[52] J.S.C. Praciano, P.S.B. Barros, E.S. Barroso, E. Parente, Á.S. de Holanda, J.B.M. Sousa, An isogeometric formulation for stability analysis of laminated plates and shallow shells, Thin-Walled Struct. 143 (2019) 106224, https://doi.org/10.1016/j.tws.2019.106224.
[53] A. Gupta, S. Verma, A. Ghosh, Static and dynamic NURBS-based isogeometric analysis of composite plates under hygrothermal environment, Compos. Struct. 284 (2022) 115083, https://doi.org/10.1016/j.compstruct.2021.115083.
[54] R. Vázquez, A new design for the implementation of isogeometric analysis in octave and matlab: GeoPDEs 3.0, Comput. Math. Appl. 72 (3) (2016) 523–554, https://doi.org/10.1016/j.camwa.2016.05.010.
[55] A. Gupta, A. Ghosh, Isogeometric static and dynamic analysis of laminated and sandwich composite plates using nonpolynomial shear deformation theory, Composites, Part B, Eng. 176 (2019) 107295, https://doi.org/10.1016/j.compositesb.2019.107295.
[56] M.K. Prabhakara, Post-buckling behaviour of simply-supported cross-ply rectangular plates, Aeronaut. Q. 27 (4) (1976) 309–316, https://doi.org/10.1017/s0001925900007812.
[57] J. Giri, G. Simitses, Deflection response of general laminated composite plates to in-plane and transverse loads, Fibre Sci. Technol. 13 (3) (1980) 225–242, https://doi.org/10.1016/0015-0568(80)90006-8.
[58] J.N. Reddy, Mechanics of Laminated Composite Plates and Shells, CRC Press, 2004.
[59] M. Ganapathi, O. Polit, M. Touratier, A c0 eight-node membrane-shear-bending element for geometrically non-linear (static and dynamic) analysis of laminates, Int. J. Numer. Methods Eng. 39 (20) (1996) 3453–3474, https://doi.org/10.1002/(sici)1097-0207(19961030)39:20 < 3453::aid-nme9 > 3.0.co;2-7.